The geochemistry and petrogenesis of the Paleoproterozoic du Chef dyke swarm, Quebec, Canada

T. Jake. R. Ciborowski*[1,2], Andrew C. Kerr[1], Iain McDonald[1], Richard E. Ernst[3], Hannah S. R. Hughes[1], and Matthew J. Minifie[1].

[1]School of Earth and Ocean Sciences, Cardiff University, Park Place, Cardiff, Wales, CF10 3AT, UK

[2]Petrolab Ltd., C Edwards Offices, Gweal Pawl, Redruth, Cornwall, TR15 3AD, UK

[3]Department of Earth Sciences, Carleton University, 1125 Colonel By Drive, Ottawa, Ontario, K1S 5B6, Canada & Ernst Geosciences, 43 Margrave Ave. Ottawa, Ontario K1T 3Y2, Canada

*email: jake.ciborowski@live.co.uk Telephone: +44 (0) 2920 876420

Abstract

The du Chef dyke swarm in southern Quebec, Canada is composed of numerous northeast trending, greenschist-amphibolite facies, gabbronoritic dykes that crop out either side of the Grenville Front. The age of the du Chef swarm (2408±3 Ga) has led previous authors to suggest a genetic link between the du Chef dykes and coeval swarms (including the Ringvassøy, Scourie, Widgemooltha and Sebanga) preserved on other Archean cratons. These now disparate dyke swarms are proposed to have formed in response to mantle plume-induced continental breakup during the early Proterozoic. This work represents the first geochemical study of the du Chef dykes and shows that the swarm evolved through fractional crystallisation of a single tholeiitic parent magma that remained largely uncontaminated during its residence and ascent through the crust. We also show that the primary magma for the du Chef swarm was derived through partial melting of an enriched region of the mantle, similar in composition to the modern-day HIMU reservoir and that the magma produced was significantly hotter than the ambient mantle at the time. We contend that the du Chef dykes are the product of early Proterozoic mantle plume magmatism and may help pinpoint an

32   ancient hotspot centre that initiated continental break up along the margin of the Superior

33   Craton at ~2.4 Ga. Other dyke swarms proposed to be genetically linked with the du Chef

34   dykes record a distinctly different petrogenetic history to that of the du Chef dykes, as

35   evidenced by their more volcanic arc-like geochemical signature. These contrasting

36   geochemical signatures in supposedly cogenetic continental tholeiitic rocks may be evidence

37   of early Proterozoic mantle heterogeneity sampled by the rising du Chef mantle plume.

38

39   **1. Introduction**

40   The du Chef dykes were first described by Cieleiski and Margole (1989) as a series of north-

41   north east trending discordant intrusions which have a maximum thickness of 30 metres and a

42   measurable strike length of up to several kilometres. The majority of the dykes crop out

43   within the Grenville Province and have been amphibolitised and otherwise deformed by

44   Grenvillian tectonism such that the igneous mineralogy is rarely preserved, being more

45   commonly altered to garnet, amphibole, plagioclase, epidote and sphene (Cieleiski and

46   Margole 1989). Krogh (1994) reports the only published age of the du Chef dykes and

47   interprets the dykes to have been emplaced at 2408±3 Ma. This age is based on U-Pb analysis

48   of two samples of magmatic zircons from a pegmatitic portion of a ~ 40 m wide

49   amphibolitised du Chef dyke that was also sampled (DC007) by this study.

50

51   Several workers have noted that the age of the du Chef dykes, and other swarms that intrude

52   the Superior Craton, overlap with those of dyke swarms preserved on the North Atlantic,

53   Karelia, Zimbabwe and Yilgarn cratons (Ernst and Buchan 2002; Kulikov et al. 2010; Pirajno

54   and Hoatson 2012). This coeval magmatism has been argued to represent the remnants of an

55   early Proterozoic Large Igneous Province (LIP) that formed during mantle plume-driven

56   breakup of an Archean supercontinent (Ernst and Buchan 2004; Söderlund et al. 2010).

57

58   This work presents the first whole-rock major and trace element data for du Chef dykes from

59   either side of the Grenville Front. These data are used to charactersise the petrogenetic

60   evolution of the swarm, investigate potential mantle sources of the primary magmas, evaluate

61   the smarms proposed mantle plume origins and, investigate potential genetic links with other

62   coeval swarms preserved on other Archean cratons.

63

64   **2. Regional Geology**

65 The Superior Craton is the largest of the Archean cratons and forms the core of the Canadian

66 Shield. It is composed of alternating, east-west trending granite-greenstone and

67 metasedimentary terranes which are commonly in fault-bounded contact with each other. The

68 granite-greenstones and intervening metasediments are widely considered to represent

69 ancient volcanic arcs and accretionary prisms that were sutured and cratonised during the late

70 Archean (e.g., Card 1990; Stachel et al. 2006). Superior Craton terranes which share a

71 common tectonic history are grouped into a number of provinces, the largest being the

72 Superior Province. On its eastern margin, the Superior Province is in fault-bounded contact

73 with the Grenville Province **(Fig. 1A)**, the latter being interpreted to be the eroded remnants

74 of a Himalayan-style continental orogen caused by the collision of Baltica and Laurentia

75 during the middle Proterozoic (Dufrechou and Harris 2013).

76

77 Near Chibougamau **(Fig. 1B)**, the Superior Province to the west of the Grenville Front is

78 composed of; (1) greenschist-facies bimodal volcanic rocks, banded iron formations and

79 cherts of the Archean Roy Group (Leclerc et al. 2011); (2) conglomerates, sandstones,

80 argillites and alkalic-shoshonitic volcanic rocks of the Archean Opemisca Group; (3) the

81 ~2.73 Ga anorthositic Lac Dorè complex and other tonalitic intrusions; and (4)

82 unconformable Proterozoic metasediments and bimodal volcanics of the Huronian

83 Supergroup (Card 1990). Close to the margin of the Superior Province, the east-west trending

84 lithotectonic boundaries of the Archean groups are deflected to the northeast before being

85 truncated at the Grenville Front. Immediately east of the Grenville Front, the dominant

86 lithotectonic trends are orientated northeast-southwest (parallel to the Grenville Front) and

87 metamorphic grade reaches amphibolite-granulite facies (Cieleiski and Margole 1989;

88 Martignole and Martelat 2005).

89

90   **3. Sample collection and petrography**

91 Given the low topographic relief and dense vegetation of southwest Quebec, sample

92 collection **(Fig. 1)** was limited to road cuts along highway 167, adjoining logging roads and a

93 few isolated whale-back type exposures **(Supplementary Figure 1A)**. In outcrop, the du

94 Chef dykes are dark green-black in colour and range in thickness from 1-2 m, up to 40 m.

95 The dykes are steeply dipping and generally trend northeast-southwest. Aside from these

96 commonalities shared by all du Chef dykes, stark differences in appearance are observed

97 between dykes from areas northwest of the Grenville Front to those preserved within the

98 Front. The most readily observed difference is the nature of the dyke margins, in that the

99   dykes from outside of the Grenville Front typically preserving very sharp and regular

100   contacts with the country rock **(Supplementary Figure 1A)** while in contrast, the margins of

101   du Chef dykes from within the Grenville Front are more irregular with the dykes appearing to

102   finger into the country rock **(Supplementary Figure 1B)**. Amphibolitised du Chef dykes

103   from within the Grenville Front also commonly preserve a foliated fabric and have

104   mineralogies characterised by occasionally abundant garnet **(Supplementary Figure 1C)**,

105   while those from outside of the Grenville Front preserve igneous textures, particularly in the

106   coarser interiors of thicker dykes **(Supplementary Figure 1D)**.

107

108   The amphibolitised du Chef dykes are generally equigranular and fine grained **(Fig. 2A)**.

109   Amphibole dominates the mineralogy of the studied samples and shows a range of crystal

110   habits from euhedral, equant prisms to anhedral, irregular forms which commonly contain

111   very fine inclusions of quartz. The next most abundant mineral is plagioclase which forms

112   irregularly shaped crystals with well-developed twins that appear to fill the spaces between

113   the amphibole crystals. Accessory phases within such amphibolitised samples include biotite

114   which tends to form elongated lath shaped crystals intergrown with the amphibole, and both

115   pyrite and magnetite which form euhedral crystals or glomerocrysts distributed throughout

116   the rock **(Fig. 2B)**.

117

118   Commonly, a planar foliation is observed in the amphibolitised du Chef dykes caused by

119   alignment of amphibole and plagioclase crystals into alternating bands **(Fig. 2C)**. In some

120   samples, porphyroblasts of garnet are preserved as medium grained, euhedral crystals

121   distributed throughout the rock **(Fig. 2D)**. Occasionally, the interiors of the garnets are filled

122   with fine grained inclusions of plagioclase, amphibole, biotite, and chlorite and often, the

123   garnets display atoll textures **(Fig. 2E)**.

124

125   In less metamorphosed samples, from northwest of the Grenville Front, primary igneous

126   minerals and textures are partially preserved. Typically, the interiors of these dykes are

127   medium grained and inequigranular **(Fig. 2F)**. The most abundant primary phase is olivine,

128   which forms euhedral relict grains that have been altered to magnesite, serpentine and iron

129   oxides, predominantly along grain boundaries and crystal fractures. Plagioclase tends to form

130   very elongate laths which appear to grow into the olivine crystals. Alteration of the

131   plagioclase is characterised by very fine grained placements of quartz and sericite

132   concentrated along crystal margins **(Fig. 2G)**. Very little primary pyroxene remains in the

133 studied samples, but its original existence of confirmed by pseudomorphic replacements by
134 calcite and amphibole.
135
136 In summary, the du Chef dykes record metamorphic mineral assemblages which range from
137 lower greenschist to upper amphibolite facies. The transition from greenschist to amphibolite
138 facies parallels the trend of the Grenville Front in this region **(Fig. 1)**. The extent to which
139 this metamorphism has affected the geochemistry of the dykes is explored in the subsequent
140 sections.
141

142 ## 4. Geochemistry

143 *4.1 Analytical procedures*
144 Sample preparation and analysis was carried out at Cardiff University. Weathered surfaces
145 and in-filled fractures were removed with a rock saw prior to analysis. The sawed samples
146 were crushed into ~5 mm chips using a steel jaw crusher and powdered in an agate planetary
147 ball mill. Approximately 2 g of the milled powder was ignited in a furnace at 900 °C for two
148 hours in order to determine loss on ignition values.
149

150 Whole-rock major element, trace element and rare earth element (REE) data were obtained
151 following Li metaborate fusion (Minifie et al. 2013). Major element and Sc abundances were
152 determined using a JY Horiba Ultima 2 Inductively Coupled Plasma Optical Emission
153 Spectrometer (ICP-OES). Trace elements were analysed by a Thermo X Series 2 Inductively
154 Coupled Plasma Mass Spectrometer (ICP-MS). International reference material JB-1A was
155 run with each sample batch to constrain the accuracy and precision of the analyses. Relative
156 standard deviations show precision of 1–5% for most major and trace elements for JB-1A. 2σ
157 values encompass certified values for the vast majority of elements. Full analytical results
158 including repeat runs of standard basalt JB-1A can be found in the Supplementary
159 Information. Representative, whole-rock major element and trace element data for the du
160 Chef dyke samples are presented in **Table 1**.
161

162 *4.2 Element mobility*
163 As the du Chef dyke swarm crops out within the Grenville Pronvince where metamorphic
164 facies reaches up to amphibolite-granulite facies (Martignole and Martelat 2005) and samples
165 show abundant alteration **(Fig. 2)**, the effects of secondary element remobilisation must be
166 considered. At metamorphic conditions above lower amphibolite facies the normally

167   immobile high field strength elements (HFSE) including the REE are expected to become

168   more mobile (Pearce 1996) and therefore any scatter observed in plots involving these

169   elements for the du Chef samples may reflect their metamorphic history. As the HFSE are

170   incompatible in the main rock forming minerals, they should plot on linear arrays when

171   plotted against each other for a suite of unaltered rocks formed from a common fractionating

172   magma, whereas secondary remobilisation of elements is likely to result in a scattered trend

173   (Cann 1970).

174

175   Good linear correlations are observed between Zr and the REE and other HFSE ($R^2 \geq 0.7$),

176   indicating that secondary remobilisation of these elements was very limited. Conversely, the

177   incompatible large ion lithophile elements (LILE) show much more scattered correlations

178   with Zr which indicates that these elements have undergone sub-solidus remobilisation. A

179   subset of these graphs is shown in **(Supplementary Figure 2)**. The following petrogenetic

180   discussion will largely be limited to using the HFSE which likely record near-primary

181   concentrations.

182

183   *4.3 Classification*

184   The total alkali silica diagram is a common way to geochemically classify igneous rocks,

185   however since Na and K have been remobilised in these dykes the total alkali silica diagram

186   cannot be used for the du Chef dykes. Instead, we use the Zr/Ti vs. Nb/Y diagram **(Fig. 3)**

187   since the elements used in this classification have been shown to have remained immobile.

188   On this diagram, the du Chef dykes plot as a fairly tight cluster within the subalkaline basalt

189   and basaltic andesite fields.

190

191   *4.4 Major elements*

192   The du Chef dykes are broadly basaltic in major element composition **(Table 1)** with, MgO

193   ranging from 5.4 to 9.0 wt.% and are relatively TiO_2 poor (1.0 to 2.7 wt.%). Na_2O, K_2O,

194   TiO_2, and MnO do not show any obvious correlation with MgO while SiO_2, Al_2O_3, and CaO

195   have positive, and P_2O_5 negative, correlations with MgO **(Supplementary Figure 3)**. Fe_2O_3

196   shows an enrichment trend characteristic of of tholeiitic magmas. The poor correlations

197   observed between the alkalis, and MgO are further evidence of element mobility in the du

198   Chef dykes while the better correlations observed between MgO, Fe_2O_3, SiO_2, Al_2O_3 and

199   CaO may suggest that the dykes evolved through the fractional crystallisation and removal of

200   olivine, clinopyroxene and plagioclase from a tholeiitic parent magma.

201

4.5 Trace elements

The du Chef dykes have relatively low concentrations of Cr and Ni **(Fig. 4)** which show positive correlations with MgO. Other compatible trace elements including Sc and V have more scattered but negative correlations with MgO. Those trace elements which are incompatible during basaltic fractionation show slightly scattered negative correlations with MgO. On similar graphs where relatively immobile Zr **(Supplementary Figure 2)** is used instead of MgO as an index of fractionation, the incompatible elements plot on much tighter, positively correlated arrays suggesting that the du Chef dykes may have formed by the fractionation of a single parent magma.

Total rare earth element (REE) abundances in the du Chef dykes range between $15 - 49 \times$ chondritic values and when plotted on chondrite-normalised REE diagrams **(Fig. 5)**, the dykes show sub-parallel trends enriched in light REE [$(La/Sm)_N = 1.9 \pm 0.3$] relative to the HREE which themselves are characterised by $(Gd/Yb)_N$ ratios of 1.31 ± 0.26. Variable but slightly positive Eu anomalies may indicate the presence of cumulate plagioclase in the magma. The enrichment of the light REE relative to the heavy REE increases with fractionation **(Supplementary Figure 4)** while the Eu anomaly becomes more negative.

5.   Modelling and discussion

5.1 Fractional crystallisation

The linear geochemical trends exhibited by the du Chef dykes suggest that the dykes evolved from a single fractionating magma. In this section, we will evaluate fractional crystallisation as a potential mechanism for generating the geochemical trends observed in the du Chef dykes. Fractional crystallisation of the most primitive du Chef dyke sample (DC011) has been modelled using the PELE computer software program (Boudreau 1999). This sample is unlikely to be a primary magma given its relatively evolved nature (~ 9 wt.% MgO), however, it represents the most primitive magma of the suite and hence, the closest estimate of the primary magma for the suite.

PELE is a Windows®-compatible computer program which allows the user to evaluate crystallisation of silicate magma at varying physical conditions. Boudreau (1999) used published descriptions of the database and numerical models used by the MELTS (Ghiorso & Sack 1995) software (currently usable as a JAVA® enabled web applet from

235   http://melts.ofm-research.org/applet.html) to produce a modified version of the program for

236   use with Windows® systems (PELE). For a detailed description of the workings of PELE, the

237   reader is referred to Ghiorso & Sack (1995), Asimow and Ghiorso (1998) and Boudreau

238   (1999). The major element geochemical trends for the du Chef dykes have been modelled

239   using six different scenarios of varying pressure and water content **(Table 2)**. All models use

240   a quartz-fayalite-magnetite (QFM) oxygen buffer and calculate the composition of the liquid

241   at 10% crystallisation intervals.

242

243   It is not entirely obvious which model best approximates the major element composition of

244   the du Chef dykes, partly due to the scatter resulting from sub-solidus element mobility, but

245   also because for certain elements (e.g., CaO and P_2O_5), the models predict similar trends

246   **(Fig. 6)**. However, high-pressure fractional crystallisation of the du Chef dyke parent magma

247   is supported by the TiO_2, SiO_2, Al_2O_3 and Fe_2O_3 compositions, the trends of which (when

248   plotted against MgO) are best approximated by models 5 (7 kbar) and 6 (10 kbar). Overall,

249   model 5, which models fractional crystallisation of a magma with a composition equal to that

250   of sample DC011 at 7 kbar, provides the most consistent fit with the du Chef dyke

251   compositions.

252

253   The 7 kbar model predicts that crystallisation of the DC011 parent magma begins at ~1261

254   °C with olivine being the first mineral to crystallise. Clinopyroxene joins olivine at ~1249 °C

255   after ~3% of the magma has crystallised. Clinopyroxene is followed by plagioclase soon after

256   at 1242 °C after ~6% of the magma has crystallised. Once the magma has cooled to 1212 °C

257   and ~44% of it has crystallised, orthopyroxene joins the crystallising assemblage before

258   leaving again once the magma cools to 1170 °C and ~65% of it has crystallised. Olivine,

259   clinopyroxene and plagioclase continue to crystallise until the magma reaches 1160 °C, at

260   which point 70% of the original parent magma has crystallised and the remaining liquid

261   contains less MgO than the most evolved du Chef dyke sampled **(Supplementary Figure 5)**.

262

263   *5.2 Crustal contamination*

264   Trace element models have been constructed to determine whether the du Chef parental

265   magma evolved via simple fractional crystallisation (FC) or through assimilation-fractional

266   crystallisation (AFC). Fractional crystallisation of the du Chef parent magma was modelled

267   using the modal mineral abundances predicted by the 7 kbar major element model and the

268   partition coefficients of Bedard (2001) using **equation 1 (see appendix)**. AFC uses the same

269   parameters as the FC model, the composition of felsic crust (Rudnick and Gao 2003) and an

270   assimilation/fractionation rate (r) of 0.1 (**equations 2** and **3**).

271

272   On primitive mantle-normalised multi-element diagrams (**Fig. 7**), the du Chef dykes show

273   similar subparallel trends to those observed on chondrite normalised REE diagrams (**Fig. 5**).

274   All of the du Chef samples show enrichments in the most incompatible elements relative to

275   the more compatible HFSE and have relative depletions in Th $[(Th/La)_N = 0.37 \pm 0.18]$. The

276   dykes also show negative Nb anomalies $(Nb_N/Nb_N^* = 0.8 \pm 0.2)$[1] and variable Ti anomalies

277      $(Ti_N/Ti_N^* = 1.1 \pm 0.5)$[2] the magnitude of which do not correlate with degree of fractionation

278   (**Supplementary Figure 4**). The du Chef dykes are further characterised by predominantly

279   negative Zr-Hf anomalies. These trace element characteristics result in the majority of the du

280   Chef dykes plotting in mantle plume-related oceanic plateau basalt fields on the Nb/Y vs.

281   Zr/Y and Zr/Nb vs. Nb/Th diagrams (**Fig. 8**).

282

283   Models which use trace elements to model FC and AFC using the parameters and

284   assemblages predicted at various degrees of crystallisation at 7 kbar are shown in **Fig. 7**. Both

285   FC and AFC models predict the general trends of increasing incompatible element

286   abundances observed in the du Chef dykes. However, the AFC model indicates that as

287   fractionation of the parent magma continues, the magmas develop an increasingly negative

288   Nb-Ta anomaly. The lack of correlation between Nb_N/Nb_N^* and Zr or MgO (used as an index

289   of fractionation) in the du Chef dykes (**Supplementary Figure 4**) shows that contamination

290   of the fractionating du Chef parent magma by felsic crust is unlikely. Instead, fractionation of

291   the du Chef dyke parent magma, with no significant input of material is our preffered

292   mechanism for explaining the trace element variation observed in the dykes. However,

293   despite the lack of systematic change in the dyke's Nb_N/Nb_N^* values, some of the scatter on

294   **Supplementary Figure 4** may be the product of in situ contamination of individual dykes by

295   heterogeneous lithologies which make up the ~10,000 km^2 area within the Grenville Province

296   (Martignole and Martelat 2005) that the du Chef dykes crop out in (**Fig. 1**).

297

298   In summary, the major element chemistry of the du Chef dykes is best explained by a model

299   that involves a body of basaltic magma containing ~9 wt.% MgO that ponded at ~21 km (~7

300   kbar) and fractionated olivine, clinopyroxene, plagioclase orthopyroxene. Trace element

---

[1] $Nb_N^* = (Th_N + La_N) / 2$
[2] $Ti_N^* = (Sm_N + Gd_N) / 2$

301 modelling indicates that during fractionation, this du Chef parent magma was not

302 contaminated by felsic country rock. Instead, the parent liquid evolved via simple fractional

303 crystallisation, over the course of which, the magma chamber was periodically tapped and

304 liquids removed to form individual du Chef dykes which record the geochemical evolution of

305 the parent magma. It is however likely that some of these evolved melts became

306 contaminated by the various crustal components into which the du Chef dyke swarm

307 intruded, thus producing some of the HFSE variation observed in **Fig. 7**.

308

309 *5.3 Primary Magmas and Mantle Source*

310 The relatively evolved nature of the du Chef dykes (MgO ≤ 9 wt.%) suggests that even the

311 most primitive dyke does not represent an unfractionated primary magma derived through

312 partial melting of mantle peridotite. To characterise the primary magmas of such evolved

313 suites, Herzberg and Asimow (2008) developed the PRIMELT2 software which can calculate

314 primary magma compositions for evolved lavas. PRIMELT2 uses forward and inverse

315 models to compute a melt fraction which is capable of, (a) being formed by partial melting of

316 fertile mantle peridotite and (b) producing the major element composition of the evolved lava

317 sample through fractionation or accumulation of olivine alone.

318

319 Fractional crystallisation models which use sample DC011 as a parent magma composition

320 predict that olivine is the first mineral to crystallise **(Supplementary Figure 5)**. This, along

321 with the ~9 wt.% MgO content of DC011, suggests that this sample could feasibly have

322 evolved solely through olivine fractionation of a primary mantle melt (Herzberg and Asimow

323 2008). Indeed, the application of PRIMELT2 to sample DC011 produces a successful result,

324 whereby the major element composition of sample DC011 can be replicated by 30% partial

325 melting of fertile mantle peridotite to produce a picritic primary magma containing 19.8 wt.%

326 MgO, 11.4 wt.% Al_2O_3 and 46.2 wt.% SiO_2 . Fractional crystallisation of this primary

327 magma, such that 32% of it crystallises as olivine, produces a remaining liquid fraction with a

328 major element composition similar to sample DC011. By using these degrees of partial

329 melting and olivine fractionation, we can investigate the possible mantle sources for the du

330 Chef dykes.

331

332 Five mantle reservoirs are modelled **(see appendix)**: Depleted MORB Mantle (DMM),

333 Enriched Mantle (EM1 and EM2) and Primitive Mantle (PM) and High $^{238}U/^{204}Pb$ Mantle

334 (HIMU). The composition of DMM has been constrained by Workman and Hart (2005) from

335 the trace element depletion trends of abyssal peridotites. The compositions of the EM1 and

336 EM2 reservoirs are estimated from inverse modelling of the compositions of EM1 and EM2

337 basalts from the Tristan da Cuhna, Gough, Samoan and Society islands (Willbold and Stracke

338 2006). The HIMU reservoir is similarly estimated from inverse modelling using the

339 compositions of basalts from Tubuai, Mangaia and Rurutu (Chauvel et al. 1992). The

340 composition of PM is derived from studies of chondritic meteorites and refractory element

341 ratios of mantle peridotites (McDonough and Sun 1995). It should be noted that projecting

342 the existence of these reservoirs, predominantly recognised from modern intraplate basaltic

343 rocks, back into the Palaeoproterozoic is questionable. However, these reservoir

344 compositions can be used to characterise the enriched or depleted nature of the du Chef

345 mantle source region.

346

347 The 30% partial melting needed to form the du Chef primary magma (as predicted by the

348 PRIMELT2 model for sample DC011) may be modelled using batch melting **(Equation 4)**

349 for garnet lherzolites (Johnson et al. 1990) from the five different mantle reservoirs described

350 above. Garnet lherzolite was chosen for the models as all of the du Chef dykes have relatively

351 depleted HREE patterns **(Fig. 5)** which indicates that mantle melting occurred within the

352 garnet stability field but was of an insufficient degree to melt all of the garnet in the source. A

353 garnet-bearing source may also be implied by the negative Zr-Hf anomalies observed in the

354 du Chef dyke, which for other intracontinental basaltic rocks, have been interpreted to have

355 been imparted on primary magmas by the segregation of magmas from a mantle plume with

356 residual majorite garnet, at depths of 400 to 600 km (Xie et al. 1993).

357

358 The PRIMELT2 model predicts that, following partial melting, 32% of the primary magma

359 crystallised as olivine, with the remaining liquid fraction approximating to the composition of

360 sample DC011. The affects of this fractionation on the trace element chemistry of the primary

361 magmas derived from the three different mantle reservoirs can be calculated using equation 1

362 and the olivine/melt partition coefficients of Bedard (2001) with 32% fractionation (F =

363 0.32).

364

365 **Fig. 9.** shows the Primitive Mantle-normalised multi-element patterns for sample DC011 for

366 which PRIMELT2.XLS was able to define partial melting and fractionation parameters. Also

367 plotted are the compositions of magmas formed by fractional crystallisation of primary

368 magmas derived from melting of garnet lherzolites from the DMM, EM1, EM2, HIMU and

369 PM mantle reservoirs using the parameters of melting and fractionation stated above. **Fig. 9.**

370 shows that a fractionated magma, derived from a primitive mantle garnet lherzolite is an

371 unlikely parent magma for the du Chef dykes as such a liquid is characterised by $(Th/La)_N =$

372 1.01- in contrast to sample DC which has a much lower ratio [$(Th/La)_N = 0.43$]. The

373 modelled fractionated magma derived from the DMM reservoir has a more similar $(Th/La)_N$

374 ratio to the du Chef dykes but also records distinctly lower trace element abundances ($2.2 \times$

375 primitive mantle) than sample DC011 ($5.4 \times$ primitive mantle). The fractionated magma

376 derived from the enriched mantle (EM1 and EM2) reservoirs have very similar element

377 abundances and primitive mantle-normalised patterns as sample DC011 for the least

378 incompatible trace elements as well as comparable $(Th/La)_N$ ratios, but fails to replicate the

379 LREE enrichment observed in the du Chef dykes [$(La/Sm)_N = 1.90 \pm 0.33$] and instead

380 showsslight LREE depletion [$(La/Sm)_N = 0.81$]. The fractionated magma derived from partial

381 melting of the HIMU reservoir records similar MREE-HREE ratios to sample DC011, but

382 predicts much higher abundances as well as contrasting $(Th/La)_N$ ratios. Further modelling

383 which involves fractionation of primary magmas formed via melting an EM1 garnet

384 lherzolite previously modified by the addition of a crustal component, [as might occur during

385 melting of lower crustal material by hot upwelling mantle (e.g., Xu et al. 2002)], is also

386 unsuccessful in replicating the trace element composition of sample DC011, since the

387 composition of the modelled magma in this instance is characterised by $(Th/La)_N$ ratios > 1

388 and negative Nb-Ta anomalies.

389

390 This indicates that fractional crystallisation of partial melts of the mantle reservoirs described

391 here is not a viable mechanism for producing the parent magma of the du Chef dykes. An

392 alternative source is suggested by the work of Polat et al. (1998) who observed similar trace

393 element characteristics in ultramafic rocks of the late-Archaean Schreiber-Hemlo and White

394 River-Dayohessarah greenstone belts of the Superior Craton. In this earlier work, Polat et al.

395 (1998) suggested that primary magmas characterised by trace element signatures like those

396 observed in the du Chef dykes were the product of deep-seated, mantle plume magmas

397 derived from subducted and recycled oceanic lithosphere albeit with a different trace element

398 signature than the HIMU reservoir modelled above.

399

400 *5.4. Thermal Plume*

401 Using overlapping U-Pb ages of mafic suites, Söderlund et al. (2010) have suggested that the

402 du Chef dyke swarm is correlative with some of the Sebanga dykes preserved on the

403   Zimbabwe craton. Söderlund et al. (2010) used this coeval geochronological data to suggest

404   that during the late-Archaean and early-Proterozoic, the Superior, Karelia and Zimbabwe

405   cratons were 'nearest neighbours' in a larger supercontinent (Ernst and Bleeker 2010;

406   Söderlund et al. 2010) which began to rift apart approximately 2.4 Ga during an episode of

407   mantle plume-driven continental breakup.

408

409   Mantle plumes active in the modern era such as those beneath Iceland and Hawaii are

410   characterised by anomalously hot upper mantle hundreds of degrees hotter than the ambient

411   mantle (Wolfe et al. 1997; Bijwaard and Spakman 1999; Li et al. 2000). For ancient

412   magmatic systems the existence of anomalously high-temperature magmatism (indicative of a

413   mantle plume) can be investigated by examining the geochemistry of primary magmas and

414   calculating their mantle potential temperature (T_P) – the temperature the mantle would reach

415   if it was brought to the surface adiabatically without melting (McKenzie and Bickle 1988).

416   The T_P of the mantle source of a primary magma may be recorded in its petrology and major

417   element geochemical composition and can be inferred by calibration and parameterisation of

418   laboratory data to the magma in question. PRIMELT2.XLS software developed by Herzberg

419   and Asimow (2008) can be used to calculate T_p. Once PRIMELT2.XLS obtains a primary

420   magma composition, the MgO concentration is used to calculate T_P where the total

421   uncertainty due to potential errors in determining the MgO content of primary magmas is $\pm$

422   60°C (2σ) (Herzberg and Asimow 2008; Herzberg et al. 2010).

423

424   PRIMELT2.XLS was able to calculate the potential temperature of 1567°C for sample

425   DC011. By comparing this potential temperature with temperature estimates of the ambient

426   upper mantle in the Palaeoproterozoic, we can determine whether the magmatism which

427   formed the du Chef dykes was derived from an anomalously hot upper mantle (i.e., plume) as

428   is predicted by the mantle plume theory (Campbell 2007), and confirmed by observations of

429   the mantle beneath Hawaii and Iceland (Bijwaard and Spakman 1999; Li et al. 2000) and

430   elsewhere (Montelli et al. 2004; Waite et al. 2006;).

431

432   There is a general consensus that the mantle was significantly hotter during the

433   Palaeoproterozoic than it is today **(Fig. 10)**. Exactly how much hotter is a contentious point

434   as different models predict different cooling histories for the Earth. Richter (1988) presents

435   models in which the starting temperature of the upper mantle at 4.5 Ga was either 2000°C or

436   2500°C which cooled at a continuously decreasing rate to reach a present day value of

437 1350°C. Regardless of the two starting temperatures used by Richter (1988), his model

438 predicts that at ~2.4 Ga the temperature of the ambient upper mantle was ~1480°C. Korenaga

439 (2008) has proposed a model which is characterised by an initial increase in mantle T_P from

440 ~1650°C at 4.5 Ga to ~1700°C at 3.6 Ga. This initial temperature increase is followed by an

441 increasingly rapid drop in T_P to a present day values of 1350°C. Davies (2009) suggests that

442 the low urey ratio (heat produced by radioactive decay/heat loss) used by Korenaga (2008) is

443 extreme and instead favours a model of constantly decreasing temperature from an initial

444 upper mantle temperature of 1800°C at 4.5 Ga to reach a modern day temperature of 1300°C.

445

446 The T_P of sample DC011 (1567°C) which yields a primary magma estimate with

447 PRIMELT2.XLS is plotted in **Fig. 10** along with the three secular cooling models described

448 above. Sample DC011 records a T_p 87°C and 179°C higher than is predicted for the ~2.4 Ga

449 mantle by the models of Richter (1988) and Davies (2009) respectively, but 138°C lower than

450 is predicted by the model of Korenaga (2008). Determining the veracity of the disparate

451 models presented in **Fig. 10** is beyond the scope of this study. However, the model of

452 Korenaga (2008) has been seriously challenged by Davies (2009) and Karato (2010). Davies

453 (2009) disagrees with the assumption of Korenaga (2008) that plate thickness is determined

454 by dehydration during melting at mid-ocean ridges and instead suggests that plate thickness is

455 determined by conductive cooling. Davies (2009) also argues that the model of Korenaga

456 (2008) is overly sensitive to the radius of curvature of bending plates at subduction zones.

457 Karato (2010) demonstrates that plate curvature at subduction zones depends on the flexural

458 rigidity which in turn, depends on plate thickness. This finding by Karato (2010) essentially

459 invalidates the model of Korenaga (2008) who assumes that the radius of curvature of

460 bending plates remains constant. On this basis therefore we prefer the models of Richter

461 (1988) and Davies (2009) in estimating the temperature of the upper mantle during the

462 emplacement of the du Chef dykes at ~2.4 Ga.

463

464 Other studies have estimated the temperature of the upper mantle at various points during the

465 Archaean (Ohta et al. 1996; Galer and Mezger 1998; Komiya et al. 2004). Galer and Mezger

466 (1998) examined the regional metamorphic grade of ten undisturbed Archaean granite-

467 greenstone segments and showed that metamorphic facies exposed at the surface today are

468 indicative of burial pressures of ~1.5 kbar. From these burial pressures, Galer and Mezger

469 (1998) infer that, since 3 Ga, the undisturbed portions of cratons have been uplifted ~5 km,

470 implying a mean continental thickness of ~46 km when the cratons were stabilised at ca. 2.5

471   Ga (Bleeker 2003). Galer and Mezger (1998) argue that during the Archaean, in order to

472   maintain isostatic equilibrium with the cratons, the oceanic crust would have had to have

473   been ~14 km thick (assuming a relatively fixed cratonic mass through time). Under these

474   conditions, Galer and Mezger (1998) infer an upper mantle temperature of ~90 °C hotter than

475   the present day at 3 Ga. Using a linear cooling rate of 30 °C Gy^{-1} (which is comparable to

476   estimates of the present day cooling rate of the Earth), the temperature of the upper mantle at

477   2.4 Ga can be estimated as 1422 °C.

478

479   Ohta et al. (1996) used the geochemistry of Archaean MORB rocks preserved in a 3.1-3.3 Ga

480   accretionary complex in Pilbara, Western Australia to constrain the ambient temperature of

481   the upper mantle at 3.1-3.3 Ga to be 1400 °C. Using this temperature of 1400 °C as an

482   estimate for T_P at 3.2 Ga and a simplistic, linear cooling modelling between 1400 °C at 3.2

483   Ga and 1350 °C today, the temperature of the mantle at 2.4 Ga can be estimated at 1387 °C.

484   In a similar study, Komiya et al. (2004) use the geochemistry of Archaean MORB rocks

485   preserved in the 3.8 Ga Isua Supracrustal Belt, southwest Greenland to constrain upper

486   mantle temperatures at that time to be ~1480 °C. Again, using a simplistic, linear cooling

487   model between 1480 °C at 3.8 Ga and 1350 °C today, the temperature of the upper mantle at

488   2.46 Ga can be estimated at 1432 °C. These three estimates of upper mantle temperature at

489   ~2.4 Ga using the work of Ohta et al. (1996), Galer and Mezger (1998) and Komiya et al.

490   (2004) are all significantly lower than the T_P recorded by sample DC011 (180 °C, 135 °C and

491   145 °C respectively). This reinforces the evidence presented by **Fig. 10** that the du Chef dyke

492   swarm formed from anomalously hot mantle plume.

493

494   In summary, secular cooling models of the Earth's mantle suggest that the du Chef dykes

495   originated from anomalously hot early-Proterozoic mantle according to the models of Davies

496   (2009) and Richter (1988) as well as other estimates derived from studies of Archaean mantle

497   rocks (Ohta et al. 1996; Galer and Mezger 1998; Komiya et al. 2004). This evidence, along

498   with consistent trace element geochemistry suggests that the du Chef dykes are be the product

499   of mantle plume-driven magmatism as proposed by Ernst and Buchan (2004) and Söderlund

500   et al. (2010). However, alternate models of the cooling of the mantle [e.g., Korenaga (2008)

501   and Abbot et al. (1994)] indicate that the du Chef dykes are not the product of an

502   anomalously hot mantle plume. Continued research into the thermal evolution of the mantle

503   and derivation of robust models which estimate the temperature of the upper mantle at ~2.4

504   Ga will help better determine the nature of the source and petrogenesis of the du Chef dykes.

505

5.5. Correlative units

506 Based on coeval U-Pb ages, other workers have proposed that the du Chef dykes may be

507 genetically linked to the 2408 ± 2 Ma (Söderlund et al. 2010) Sebanga dykes preserved on the

508 Zimbabwe craton, as well as potentially to the 2403 ± 3 Ma (Kullerud et al. 2006)

509 Ringvassoy dykes (Kola-Karelia craton), 2410 ± 2 Ma (Doehler and Heaman 1998)

510 Widgiemooltha swarm and the 2418 ± 3 Ma (Nemchin and Pidgeon 1998) Scourie dyke

511 swarm. These other igneous provinces, comprised of numerous, predominantly doleritic

512 intrusions are similar to the du Chef dyke swarm in terms of areal extent and their continental

513 tholeiitic basalt geochemical affinities (Kullerud et al. 2006; Hughes et al. submitted).

514 Together with the du Chef dyke swarm, these suites may represent a hitherto unknown early

515 Proterozoic Large Igneous Province (Ernst and Buchan 2002).

516

517 Comparisons of the trace element geochemistry of the du Chef dykes and their potential

518 correlative suites **(Fig. 11)** for which such data exists in the literature allow for some

519 interesting observations to be made. Firstly, there is a striking similarity between all of the

520 suites in terms of their general enrichments in the most incompatible REE relative to the least

521 incompatible elements. Of the three suites potentially correlative with the du Chef swarm, it

522 is the Scourie dykes which have the most similar trace element geochemistry to the du Chef

523 dykes. These two dyke swarms share comparable average trace element abundances as well

524 as similarly large Zr-Hf and Y anomalies, which may indicate the two swarms were derived

525 from a common mantle reservoir that underwent a similar degree of partial melting.

526 However, in contrast to the du Chef dykes, both the Ringvassoy and Scourie dykes all have

527 high $(Th/La)_N$ ratios and are characterised by significant, negative Nb-Ta anomalies.

528

529 The trace element signatures of these three suites are common in igneous rocks formed in

530 modern volcanic arc settings (e.g., Pearce and Peate 1995). Thus, when observed in

531 palaeoproterozoic igneous rocks, these signatures have often been interpreted as evidence of

532 formation in such an environment (e.g., Van Boening and Nabelek 2008). However, the

533 volcanic arc-like trace element compositions recorded by the du Chef dykes are common in

534 the palaoeproterozoic igneous record and are observed in rocks of a similar age which

535 preserve field evidence that entirely precludes a subduction-related setting including radiating

536 dyke swarms and flood basalt provinces (Phinney and Halls 2001; Jolly 1987). For such

537 suites which record trace element signatures like those observed in the dykes potentially

539 correlative with du Chef, alternative petrogenetic mechanisms which may impart an arc-like
540 trace element geochemistry have been suggested. Potential explanations include; (1) partial
541 melting of subduction-modified sub-continental lithospheric mantle (Sandeman and Ryan
542 2008); (2) a widespread ancient mantle reservoir, fundamentally different to those observed
543 in the modern mantle (Vogel et al. 1998); or, (3) the contamination of mantle melts by
544 continental crust during fractionation in deep crustal magma chambers (e.g., Nelson et al.
545 1990).
546
547 Thus the differences in the trace element chemistry observed between the du Chef swarm and
548 its potential correlative suites do not necessarily rule out a cogenetic origin. Instead, these
549 differences may be the product of melting of a compositionally heterogeneous mantle plume
550 head that had sampled various mantle reservoirs or lithospheric components during its transit
551 through the crust and mantle, (cf., Kerr et al. 2002; Ketchum et al. 2013) or potentially
552 through the mutual evolution of cogenetic mantle melts in disparate crustal magma chambers
553 (Bleeker 2004). Further work aimed at better defining the ages of these coeval suites would
554 better constrain any potential temporal link, while further palaeomagnetic work would
555 characterise the possibility of a 'nearest neighbour' situation (Bleeker 2003) between the
556 suites at ~2.4 Ga **(Fig. 12)**.
557

558 **6.   Summary and conclusions**
559
560   1. The primary magma of the du Chef was a low-Ti, low-Al picritic basalt, derived from
561   partial melting of a garnet-bearing mantle peridotite similar in trace element
562   composition (but more enriched) to the modern-day HIMU reservoir.
563   2. The magma produced by this partial melting was significantly higher in temperature
564   than the ambient mantle and may indicate the presence of a mantle plume beneath the
565   Superior craton during the early Proterozoic.
566   3. Prior to intrusion of the dykes, the du Chef primary magma ponded in a mid-deep
567   level crustal chamber where it fractionated olivine, clinopyroxene, plagioclase and
568   orthopyroxene but with little assimilation of host rocks. This mid-deep level crustal
569   chamber was periodically tapped, with fractions of melt migrating from the chamber
570   to be emplaced as individual du Chef dykes.
571   4. Individual dykes were contaminated insitu by the host rocks and inherited variable,
572   but minor, negative anomalies in some of the HFSE.

573   5. Units proposed to be correlative with the du Chef dykes have slightly different
574   geochemical compositions that may be the result of differences in source reservoir or
575   contamination by crust or lithospheric mantle

576

583

584 **8. References**

585

586 Abbott, D., Burgess, L., Longhi, J. and Smith W. H. F., 1994. An empirical thermal history of the Earth's upper
587   mantle. *Journal of Geophysical Research*, 99, 13835–13850

588 Asimow, P. D., and Ghiorso, M. S., 1998. Algorithmic modifications extending MELTS to calculate subsolidus
589   phase relations. *American Mineralogist,* 83, 1127–1132.

590 Bédard, J., 2001. Parental magmas of the Nain Plutonic Suite anorthosites and mafic cumulates: a trace element
591   modelling approach. *Contributions to Mineralogy and Petrology,* 141**,** 747-771.

592 Bijwaard, H. and Spakman, W., 1999. Tomographic evidence for a narrow whole mantle plume below Iceland.
593   *Earth and Planetary Science Letters,* 166**,** 121-126.

594 Bleeker, W., 2003. The late Archean record: a puzzle in ca. 35 pieces. *Lithos,* 71**,** 99-134.

595 Bleeker, W., 2004. Taking the pulse of planet Earth: a proposal for a new multi-disciplinary flagship project in
596   Canadian solid Earth sciences. *Geoscience Canada,* 31**,** 179-190.

597 Boudreau, A. E., 1999. PELE-a version of the MELTS software program for the PC platform. *Comput. Geosci.,*
598   25**,** 201-203.

599 Campbell, I. H., 2007. Testing the plume theory. *Chemical Geology,* 241**,** 153-176.

600 Cann, J. R., 1970. Rb, Sr, Y, Zr and Nb in some ocean floor basaltic rocks. *Earth and Planetary Science Letters,*
601   10**,** 7-11.

602 Card, K. D., 1990. A review of the Superior Province of the Canadian Shield, a product of Archean accretion.
603   *Precambrian Research,* 48**,** 99-156.

604 Chauvel, C., Hofmann, A. W. and Vidal, P., 1992. HIMU-EM: The French Polynesian connection. *Earth and*
605   *Planetary Science Letters,* 110**,** 99-119.

606 Ciesielski, A. 1991. Litho-tectonic map of the Grenville Front, southeast of Val d'Or, Quebec. In *Open File*.
607   Geological Survey of Canada.

608 Condie, K.C., 2005. High field strength element ratios in Archean basalts - a window to evolving sources of
609   mantle plumes? *Lithos*, 79, 491-504.

610   Davies, G. F., 2009. Effect of plate bending on the Urey ratio and the thermal evolution of the mantle. *Earth and*
611   *Planetary Science Letters,* 287**,** 513-518.

612   DePaolo, D.J., 1981. Trace element and isotopic effects of combined wallrock assimilation and fractional
613   crystallization: *Earth and Planetary Science Letters*, 53, 189-202.

614   Doehler, J.S., and Heaman L.M., 1998. 2.41 Ga U–Pb baddeleyite ages for two gabbroic dykes from the
615   Widgiemooltha Swarm, Western Australia. A Yilgarn–Lewisian connection? *Geological Society of*
616   *America 1998 Annual Meeting, Abstracts with Programs, Geological Society of America,* 30, 291–292.

617   Dufrechou, G.; Harris, L.B., 2013.Tectonic models for the origin of regional transverse structures in the
618   Grenville Province of SW Quebec interpreted from regional gravity. *Journal of Geodynamics* 64, 15-
619   39.

620   Ernst, R. E. and Buchan, K. L., 2002. Maximum size and distribution in time and space of mantle plumes:
621   evidence from large igneous provinces. *Journal of Geodynamics,* 34 309-342.

622   Ernst, R. E. and Buchan, K. L., 2004. Large Igneous Provinces (LIPs) in Canada and adjacent regions: 3 Ga to
623   Present. *Geoscience Canada,* 31**,** 103-126.

624   Ernst, R. E. and Bleeker, W., 2010. Large igneous provinces (LIPs), giant dyke swarms, and mantle plumes:
625   significance for breakup events within Canada and adjacent regions from 2.5 Ga to the Present.
626   *Canadian Journal of Earth Sciences,* 47**,** 695-739.

627   Galer, S. J. G. and Mezger, K., 1998. Metamorphism, denudation and sea level in the Archean and cooling of
628   the Earth. *Precambrian Research,* 92**,** 389-412.

629   Ghiorso, M. S. and Sack, R. O., 1995. Chemical mass transfer in magmatic processes IV. A revised and
630   internally consistent thermodynamic model for the interpolation and extrapolation of liquid-solid
631   equilibria in magmatic systems at elevated temperatures and pressures. *Contributions to Mineralogy*
632   *and Petrology,* 119**,** 197-212.

633   Herzberg, C. and Asimow, P. D., 2008. Petrology of some oceanic island basalts: PRIMELT2.XLS software for
634   primary magma calculation. *Geochem. Geophys. Geosyst.,* 9**,** Q09001.

635   Herzberg, C., Condie, K. and Korenaga, J., 2010. Thermal history of the Earth and its petrological expression.
636   *Earth and Planetary Science Letters,* 292**,** 79-88.

637   Hughes, H. S. R., McDonald, I., Goodenough, K. M., Kerr, A. C. and Ciborowski, T. J. R., (submitted).
638   Geochemistry of the Scourie Dyke Suite: Evidence for parental magma sources and insights into the
639   Lewisian lithospheric mantle, NW Scotland, *Lithos*

640   Johnson, K. T. M., Dick, H. J. B. and Shimizu, N., 1990. Melting in the oceanic upper mantle: an ion
641   microprobe study of diopsides in abyssal peridotites. *Journal of Geophysical Research,* 95**,** 2661-2678.

642   Jolly, W. T., 1987. Geology and geochemistry of Huronian rhyolites and low-Ti continental tholeiites from the
643   Thessalon region, central Ontario. *Canadian Journal of Earth Sciences,* 24**,** 1360-1385.

644   Karato, S.-i., 2010. Rheology of the deep upper mantle and its implications for the preservation of the
645   continental roots: A review. *Tectonophysics,* 481**,** 82-98.

646   Kerr, A. C., Tarney, J., Kempton, P. D., Spadea, P., Nivia, A., Marriner, G. F. and Duncan, R. A., 2002.
647   Pervasive mantle plume head heterogeneity: Evidence from the late Cretaceous Caribbean-Colombian
648   oceanic plateau. *Journal of Geophysical Research: Solid Earth,* 107**,** ECV 2-1-ECV 2-13.

649   Ketchum K. Y., Heaman L. M., Bennett G., and Hughes, D., 2013. Age, petrogenesis and tectonic setting of the
650   Thessalon volcanic rocks, Huronian Supergroup, Canada. *Precambrian Research,* 233, 144-172.

651   Komiya, T., Maruyama, S., Hirata, T., Yurimoto, H. and Nohda, S., 2004. Geochemistry of the oldest MORB
652   and OIB in the Isua Supracrustal Belt, southern West Greenland: Implications for the composition and
653   temperature of early Archean upper mantle. *Island Arc,* 13**,** 47-72.

654   Korenaga, J., 2008. Urey ratio and the structure and evolution of Earth's mantle. Reviews of Geophysics, 46, 1-
655   32.

656   Kullerud, K., Skjerlie, K. P., Corfu, F. and de la Rosa, J.D., 2006. The 2.40 Ga Ringvassøy mafic dykes, West
657   Troms Basement Complex, Norway: The concluding act of early Palaeoproterozoic continental
658   breakup. *Precambrian Research*, 150, 183-200.

659   Krogh, T. E., 1994. Precise U-Pb ages for Grenvillian and pre-Grenvillian thrusting of Proterozoic and Archean
660   metamorphic assemblages in the Grenville Front tectonic zone, Canada. *Tectonics,* 13**,** 963-982.

661   Kulikov, V. S., Bychkova, Y. V., Kulikova, V. V. and Ernst, R., 2010. The Vetreny Poyas (Windy Belt)
662   subprovince of southeastern Fennoscandia: An essential component of the ca. 2.5–2.4 Ga
663   Sumian large igneous provinces. *Precambrian Research,* 183**,** 589-601.

664   Leclerc, F., Bédard, J. H., Harris, L. B., McNicoll, V. J, Goulet, N., Roy, P., and Houle., 2011. Tholeiitic to
665   calc-alkaline cyclic volcanism in the Roy Group, Chibougamau area, Abitibi Greenstone Belt —
666   revised stratigraphy and implications for VHMS exploration. *Canadian Journal of Earth Sciences*, 48,
667   661-694.

668   Li, X., Kind, R., Priestley, K., Sobolev, S. V., Tilmann, F., Yuan, X. and Weber, M., 2000. Mapping the
669   Hawaiian plume conduit with converted seismic waves. *Nature,* 405**,** 938-941.

670   Martignole, J. and Martelat, J.-E., 2005. Proterozoic mafic dykes as monitors of HP granulite facies
671   metamorphism in the Grenville Front Tectonic Zone (western Quebec). *Precambrian Research,* 138**,**
672   183-207.

673   McDonough, W. F. and Sun, S. S., 1995. The composition of the Earth. *Chemical Geology,* 120**,** 223-253.

674   Minifie, M. J., Kerr, A. C., Ernst, R. E., Hastie, A. R., Ciborowski, T. J. C., Desharnais, G. and Milliar, I. L.,
675   2013. The northern and southern sections of the western ca. 1880 Ma Circum-Superior Large Igneous
676   Province, North America: The Pickle Crow dyke connection? *Lithos*, 174, 217-235.

677   Montelli, R., Nolet, G., Dahlen, F. A., Masters, G., Engdahl, E. R., and Hung, S-H., 2004. Finite-Frequency
678   Tomography Reveals a Variety of Plumes in the Mantle. Science, 16, 338-343.

679   Nelson, D. O., Morrison, D. A. and Phinney, W. C., 1990. Open-system evolution versus source control in
680   basaltic magmas: Matachewan-Hearst dike swarm, Superior Province, Canada. *Canadian Journal of*
681   *Earth Sciences,* 27, 767-783.

682   Nemchin, A. A. and Pidgeon, R. T., 1998. Precise conventional and SHRIMP baddeleyite U-Pb age for the
683   Binneringie Dyke, near Narrogin, Western Australia, *Australian Journal of Earth Sciences*, 45, 673-
684   675.

685   Ohta, H., Maruyama, S., Takahashi, E., Watanabe, Y. and Kato, Y., 1996. Field occurrence, geochemistry and
686   petrogenesis of the Archean Mid-Oceanic Ridge Basalts (AMORBs) of the Cleaverville area, Pilbara
687   Craton, Western Australia. *Lithos,* 37**,** 199-221.

688 Pearce, J. A., 1996. A user's guide to basalt discrimination diagrams. In *Trace element geochemistry of volcanic*
689 *rocks: appliction for massive sulphide exploration,* ed. D. Wyman, 79-113. Winnipeg: Geological
690 Association of Canada, Mineral Deposits Division.

691 Pearce, J. A. and Peate, D. W., 1995. Tectonic implications of the composition of volcanic arc magmas *Annual*
692 *review of Earth and planetary sciences,* 23**,** 251-285.

693 Phinney, W. C. and Halls, H. C., 2001. Petrogenesis of the Early Proterozoic Matachewan dyke swarm, Canada,
694 and implications for magma emplacement and subsequent deformation. *Canadian Journal of Earth*
695 *Sciences,* 38**,** 1541-1563.

696 Polat, A., Kerrich, R., and Wyman, D. A., 1998. The late Archean Schreiber-Hemlo and White River-
697 Dayohessarah greenstone belts, Superior Province: Collages of oceanic plateaus, Oceanic island arcs,
698 and subduction-accretion complexes. *Tectonophysics* 289, 295-326.

699 Pirajno, F. and Hoatson, D.M., 2012. A review of Australia's Large Igneous Provinces and associated mineral
700 systems: Implications for mantle dynamics through geological time. *Ore Geology Reviews* 48, 2-54.

701 Richter, F. M., 1988. A Major Change in the Thermal State of the Earth at the Archean-Proterozoic Boundary:
702 Consequences for the Nature and Preservation of Continental Lithosphere. *Journal of Petrology,*
703 Special_Volume**,** 39-52.

704 Rudnick, R. L. and Gao, S., 2003. 3.01 - Composition of the Continental Crust. In *Treatise on Geochemistry,*
705 eds. D. H. Editors-in-Chief: Heinrich and K. T. Karl, 1-64. Oxford: Pergamon.

706 Sandeman, H. A. and Ryan, J. J., 2008. The Spi Lake Formation of the central Hearne domain, western
707 Churchill Province, Canada: an axial intracratonic continental tholeiite trough above the cogenetic
708 Kaminak dyke swarm. *Canadian Journal of Earth Sciences,* 45**,** 745-767.

709 Söderlund, U., Hofmann, A., Klausen, M. B., Olsson, J. R., Ernst, R. E. and Persson, P.-O., 2010. Towards a
710 complete magmatic barcode for the Zimbabwe craton: Baddeleyite U–Pb dating of regional dolerite
711 dyke swarms and sill complexes. *Precambrian Research,* 183**,** 388-398.

712 Stachel, T., Banas, A., Muehlenbachs, K., Kurszlaukis, S. and Walker, E.C., 2006. Archean diamonds from
713 Wawa (Canada): samples from deep cratonic roots predating cratonization of the Superior Province.
714 *Contributions to Mineralogy and Petrology*, 151, 737-750.

715 Sun, S. –s., McDonough, W. F., 1989. Chemical and isotopic systematics of oceanic basalts: implications for
716 mantle composition and processes, *Geological Society, London, Special Publications*, 42, 313-345.

717 Thériault, R., Beauséjour, S. and Tremblay, A., 2012. MAP: Geology of Québec DV2012-7. Ministère des
718 Ressources naturelles. Direction générale de Géologie Québec

719 Van Boening, A. M. and Nabelek, P. I., 2008. Petrogenesis and tectonic implications of paleoproterozoic mafic
720 rocks in the Black Hills, South Dakota. *Precambrian Research,* 167**,** 363-376.

721 Vogel, D. C., Vuollo, J. I., Alapieti, T. T. and James, R. S., 1998. Tectonic, stratigraphic, and geochemical
722 comparisons between ca. 2500-2440 Ma mafic igneous events in the Canadian and Fennoscandian
723 Shields. *Precambrian Research,* 92**,** 89-116.

724 Waite, G. P., Smith, R. B. and Allen, R. M., 2006. V_P and V_S structure of the Yellowstone hot spot from
725 teleseismic tomography: Evidence for an upper mantle plume. *Journal of Geophysical Research*, 111,
726 B04303.

727   Willbold, M. and Stracke, A., 2006. Trace element composition of mantle end-members: Implications for
728   recycling of oceanic and upper and lower continental crust. *Geochem. Geophys. Geosyst.,* 7**,** Q04004.

729   Wolfe, C. J., Bjarnason, I. T., VanDecar, J. C. and Solomon, S. C., 1997. Seismic structure of the Iceland mantle
730   plume. *Nature,* 385, 245-247.

731   Workman, R. K. and Hart, S. R., 2005. Major and trace element composition of the depleted MORB mantle
732   (DMM). *Earth and Planetary Science Letters,* 231, 53-72.

733   Xie, Q., Kerrich, R. and Fan, J., 1993. HFSE/REE fractionations recorded in three komatiite-basalt sequences,
734   Archean Abitibi greenstone belt: Implications for multiple plume sources and depths. *Geochimica et*
735   *Cosmochimica Acta,* 57, 4111-4118.

736   Xu, J-F., Shinjo, R., Defant, M. J., Wang, Q. and Rapp, R. P., 2002. Origin of Mesozoic adakitic intrusive rocks
737   in the Ningzhen area of east China: Partial melting of delaminated lower continental crust? *Geology*,
738   30, 1111-1114.

739

Manuscript Tables

Sample	DC001	DC002	DC003	DC004	DC005	DC006	DC007	DC008	DC010	DC011	DC013	DC014	DC015	DC016	DC017	DC018	DC019	DC020
UTM (E)	550620	550653	560353	565583	573015	573462	548834	552965	552965	585722	584705	584680	581748	578738	578768	582583	582578	582595
UTM (N)	5497068	5497125	5479443	5471571	5467189	5466863	5463730	5458295	5458295	5459991	5460291	5460299	5468324	5481228	5481245	5482545	5482500	5483019
Majors (wt.%)																		
SiO_2	45.57	47.40	45.04	47.88	52.01	47.13	47.82	47.43	45.90	47.60	48.13	46.15	45.70	45.32	45.69	48.03	47.82	48.06
TiO_2	2.38	1.62	2.47	1.54	1.02	1.66	1.61	1.33	1.30	1.17	1.17	1.58	2.60	2.69	2.20	1.11	1.20	1.46
Al_2O_3	14.40	14.35	13.50	14.70	14.41	15.65	13.28	15.69	15.52	15.33	13.79	14.56	13.97	12.34	14.12	15.25	15.47	15.69
Fe_2O_3	15.94	14.88	18.56	14.38	12.20	14.16	16.21	12.03	12.32	11.92	14.66	16.56	17.70	19.68	17.61	14.00	14.74	13.01
MnO	0.22	0.20	0.23	0.19	0.17	0.17	0.22	0.15	0.18	0.15	0.19	0.20	0.22	0.23	0.21	0.18	0.19	0.16
MgO	5.73	6.04	5.37	6.39	5.95	7.23	6.29	7.87	8.04	9.02	6.40	6.76	5.76	7.13	5.87	8.88	7.42	6.82
CaO	9.92	9.63	8.55	9.45	9.81	9.85	8.99	10.34	10.50	11.66	10.38	9.40	9.27	9.99	9.24	10.05	10.10	9.65
Na_2O	2.38	2.14	2.75	2.55	2.46	3.25	2.78	2.53	2.42	2.26	2.45	2.37	2.19	2.18	2.23	2.17	2.20	2.64
K_2O	1.21	1.10	1.20	0.85	0.91	0.58	0.95	0.70	1.26	0.35	0.64	0.67	0.92	0.56	0.63	0.36	0.34	0.55
P_2O_5	0.31	0.30	0.27	0.19	0.07	0.22	0.38	0.15	0.15	0.14	0.17	0.21	0.42	0.21	0.28	0.10	0.12	0.18
LOI	1.58	1.48	1.27	0.89	0.82	1.21	0.57	1.66	2.21	1.36	0.71	0.93	1.54	0.42	1.93	0.25	0.47	0.55
Total	99.64	99.12	99.21	99.01	99.84	101.13	99.09	99.88	99.80	100.95	98.69	99.40	100.29	100.74	100.03	100.38	100.05	98.76
Traces (ppm)																		
Sc	37.3	39.2	40.9	39.5	41.0	29.7	35.2	26.1	25.5	27.5	46.0	35.9	35.8	49.2	32.5	35.0	36.9	27.0
Zr	156.1	135.9	131.5	67.7	54.6	89.0	161.7	82.1	88.4	67.3	69.0	64.7	148.9	87.9	115.4	50.7	49.7	92.6
V	325.6	262.1	398.1	225.9	241.4	203.8	161.2	177.0	180.1	177.7	202.7	232.5	256.4	391.5	221.2	203.6	226.0	219.2
Cr	97.9	106.9	42.6	118.3	153.1	89.5	117.4	186.6	179.3	228.1	134.3	76.0	168.9	205.5	70.5	202.6	108.7	95.2
Co	52.4	49.9	56.5	50.4	41.3	57.1	52.2	50.0	46.0	47.0	53.0	61.5	52.6	61.3	54.7	59.8	54.3	49.6
Ni	72.3	81.4	109.7	137.3	121.5	121.9	78.1	171.8	185.5	186.5	52.3	92.6	411.9	133.1	81.3	430.4	116.0	123.3
Cu	92.0	80.9	106.6	88.8	94.5	77.3	78.4	74.0	57.6	55.9	75.7	85.2	88.1	109.5	88.4	82.4	99.4	78.1
Ga	20.5	18.3	21.9	18.0	15.8	18.1	18.9	17.7	16.5	16.2	17.5	18.0	20.2	19.3	20.7	15.6	17.2	18.6
Rb	30.1	25.9	20.0	7.1	19.7	9.5	15.9	5.5	18.5	9.9	8.3	5.7	14.5	7.9	9.7	5.6	4.8	10.0
Sr	260.5	217.9	242.9	298.6	173.0	325.8	258.4	306.1	233.6	293.0	246.7	257.3	236.6	234.4	260.1	225.5	228.7	321.6
Y	31.8	27.2	31.9	26.4	22.2	23.9	40.1	20.0	20.5	17.2	24.1	26.2	43.4	29.1	33.1	18.7	20.1	21.5
Nb	9.47	5.33	9.48	4.55	3.40	7.15	11.54	5.89	5.70	4.73	3.59	3.49	12.93	6.43	8.90	3.34	3.29	6.45
La	17.12	12.29	14.11	8.24	5.81	10.51	19.61	10.31	7.90	7.56	7.82	9.42	20.10	9.16	12.89	5.67	6.30	11.14
Ce	38.44	27.68	30.87	17.48	10.59	23.69	43.00	19.72	18.22	15.80	17.48	18.75	38.29	21.22	29.56	12.22	12.88	22.23
Pr	5.15	3.82	4.31	2.56	1.59	3.32	5.86	2.74	2.52	2.23	2.47	2.71	5.23	3.04	4.12	1.71	1.84	3.02
Nd	22.39	17.01	19.10	11.59	7.41	14.64	25.68	11.99	11.55	10.15	11.55	12.59	23.28	14.17	18.32	7.93	8.70	13.57
Sm	5.23	4.07	4.79	3.06	2.32	3.59	6.25	3.11	3.05	2.67	3.18	3.37	5.83	3.76	4.66	2.22	2.53	3.49
Eu	1.76	1.60	1.76	1.23	0.86	1.32	2.07	1.11	1.06	0.94	1.22	1.31	1.91	1.49	1.72	0.89	2.90	1.24
Gd	5.29	4.20	4.92	3.29	2.57	3.69	6.30	3.16	3.11	2.66	3.28	3.45	6.01	3.98	4.73	2.36	2.64	3.46
Tb	0.86	0.70	0.83	0.59	0.48	0.60	1.05	0.53	0.55	0.46	0.58	0.62	1.05	0.70	0.82	0.43	0.48	0.59
Dy	5.19	4.41	5.14	3.88	3.19	3.68	6.36	3.21	3.43	2.74	3.76	3.94	6.59	4.44	5.16	2.89	3.07	3.60
Ho	0.99	0.85	0.98	0.77	0.63	0.69	1.22	0.60	0.63	0.52	0.74	0.77	1.29	0.86	0.99	0.57	0.61	0.67
Er	2.72	2.39	2.73	2.16	1.78	1.93	3.34	1.64	1.74	1.45	2.12	2.21	3.67	2.46	2.86	1.65	1.78	1.84
Tm	0.43	0.38	0.43	0.35	0.30	0.30	0.54	0.26	0.27	0.22	0.34	0.35	0.59	0.38	0.45	0.27	0.29	0.29
Yb	2.91	2.59	2.94	2.37	2.02	1.98	3.57	1.67	1.74	1.43	2.22	2.33	3.87	2.55	2.96	1.76	1.96	1.91
Lu	0.44	0.41	0.45	0.37	0.30	0.30	0.54	0.25	0.25	0.21	0.33	0.35	0.59	0.38	0.44	0.27	0.30	0.29
Hf	3.72	3.14	3.18	1.85	1.54	2.27	3.77	2.17	2.11	1.74	1.93	1.78	3.94	2.35	3.08	1.47	1.41	2.27
Ta	0.68	0.36	0.62	0.32	0.23	0.48	0.81	0.41	0.40	0.33	0.24	0.23	0.88	0.44	0.60	0.22	0.23	0.46
Pb	4.11	4.57	10.32	4.12	4.07	5.44	4.82	5.58	7.76	2.20	2.22	3.06	4.31	2.60	2.20	0.64	31.91	1.52
Th	1.16	0.72	0.60	0.33	0.38	0.59	0.83	0.58	0.51	0.41	0.30	0.23	1.19	0.43	0.73	0.27	0.22	0.61
U	0.29	0.20	0.22	0.18	0.18	0.15	0.24	0.16	0.16	0.12	0.08	0.07	0.31	0.10	0.18	0.07	0.12	0.17

Table 1. Geochemical data for the du Chef dykes studied

Model	Pressure	H_2O content	Oxygen buffer
Model 1	1 kbar	0%	QFM
Model 2	1 kbar	1%	QFM
Model 3	3 kbar	0%	QFM
Model 4	5 kbar	0%	QFM
Model 5	7 kbar	0%	QFM
Model 6	10 kbar	0%	QFM

Table 2. Model parameters used in Pele for investigation fractional crystallisation of sample DC011

Trace element (ppm)	Mantle Reservoirs			Components used in reservoir construction				
	DMM	EM1	Primitive Mantle	Lower crust	Oceanic crust	N-MORB	Altered MORB	Gabbro
Th	0.008	0.029	0.085	1.200	0.106	0.120	0.193	0.078
Nb	0.149	0.376	0.713	5.000	2.136	2.330	3.563	1.695
Ta	0.010	0.027	0.041	0.270	0.173	0.132	0.246	0.192
La	0.192	0.596	0.687	8.000	3.813	2.500	4.181	4.790
Ce	0.550	1.753	1.775	20.000	11.753	7.500	13.083	14.890
Pr	0.107	0.288	0.276	2.400	1.858	1.320	2.309	2.199
Nd	0.581	1.466	1.354	11.000	9.254	7.300	12.236	10.220
Zr	5.1	12.6	11.2	68.0	81.1	74.0	127.4	77.6
Hf	0.157	0.359	0.309	1.900	2.212	2.050	3.334	2.118
Sm	0.239	0.517	0.444	2.800	3.041	2.630	4.439	3.090
Eu	0.096	0.199	0.168	1.100	1.134	1.020	1.533	1.145
Ti	716	1433	1300	4916	8212	7600	11498	8045
Gd	0.358	0.716	0.596	3.100	4.029	3.680	6.283	3.858
Tb	0.070	0.134	0.108	0.480	0.738	0.670	1.054	0.730
Dy	0.505	0.922	0.737	3.100	4.854	4.550	6.996	4.669
Y	3.33	5.77	4.55	16.00	29.06	28.00	44.13	26.89
Ho	0.115	0.204	0.164	0.680	1.040	1.010	1.570	0.957
Er	0.35	0.60	0.48	1.90	3.01	2.97	4.38	2.77
Tm	0.054	0.092	0.074	0.240	0.459	0.456	0.656	0.421
Yb	0.365	0.616	0.493	1.500	3.028	3.050	4.240	2.767
Lu	0.058	0.095	0.074	0.250	0.451	0.455	0.675	0.402

Table 3. Trace element compositions of mantle reservoirs used in this study. See text for description of data.
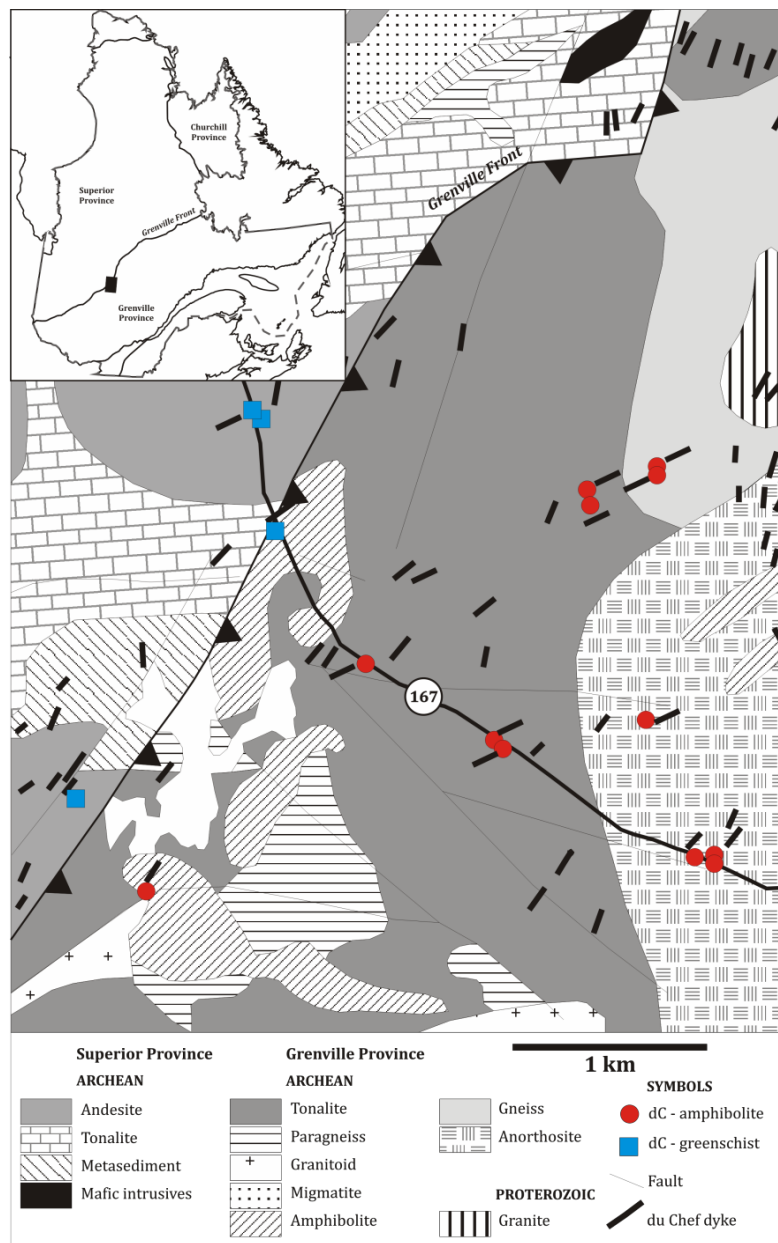
Fig. 1. Geological map of area showing sample locations. Geology modified after Thériault et al. (2012).
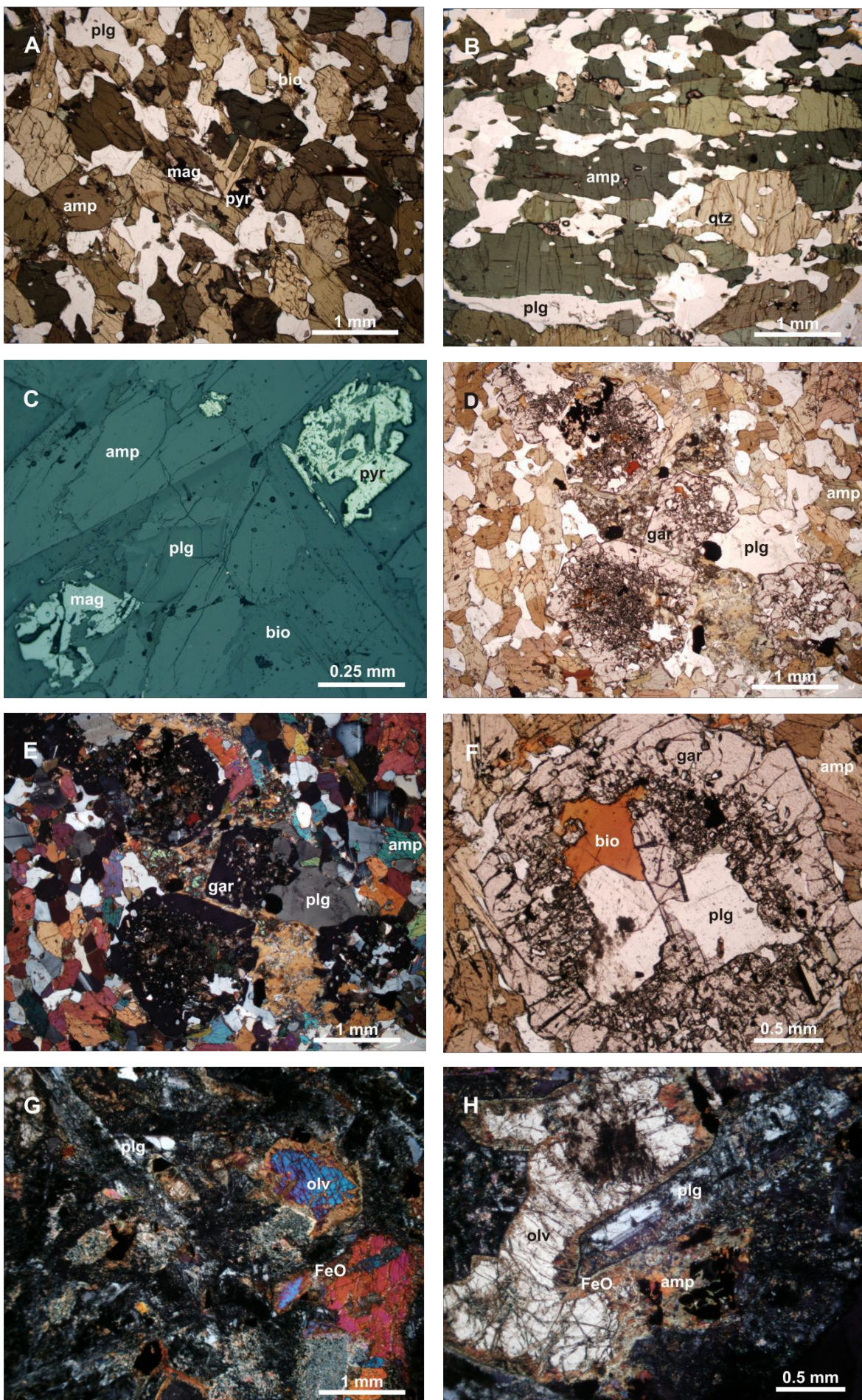
Fig 2. Photomicrographs of the du Chef dykes: A – general view of non-foliated amphibolite samples; B – general view of foliated amphibolite samples; C – reflected light micrograph showing textures of magnetite and pyrite in amphibolite samples; D – garnet porphyroblasts; E – crosspolarised view of D; F – garnet porphyroblast showing atoll texture; G – general view of non-amphibolitised du Chef dyke; H – alteration of olivine and plagioclase in non-amphibolitised dykes. Abbreviations: amp – amphibole, bio – biotite, plg – plagioclase, mag – magnetite, pyr – pyrite, qtz – quartz, gar – garnet.
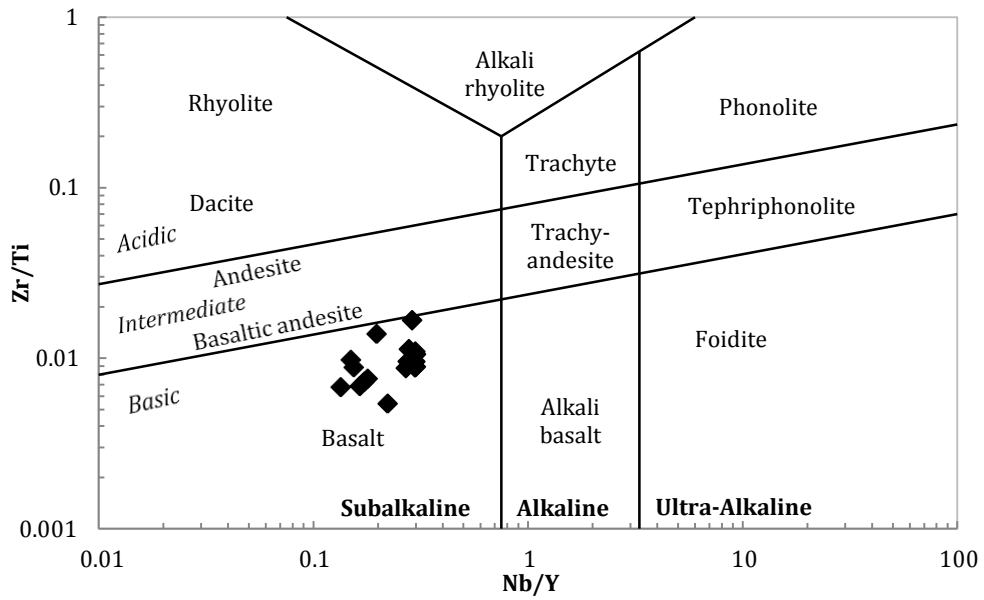
Fig. 3. Zr/Ti vs. Nb/Yb classification diagram (Pearce 1996) for the du Chef dykes.
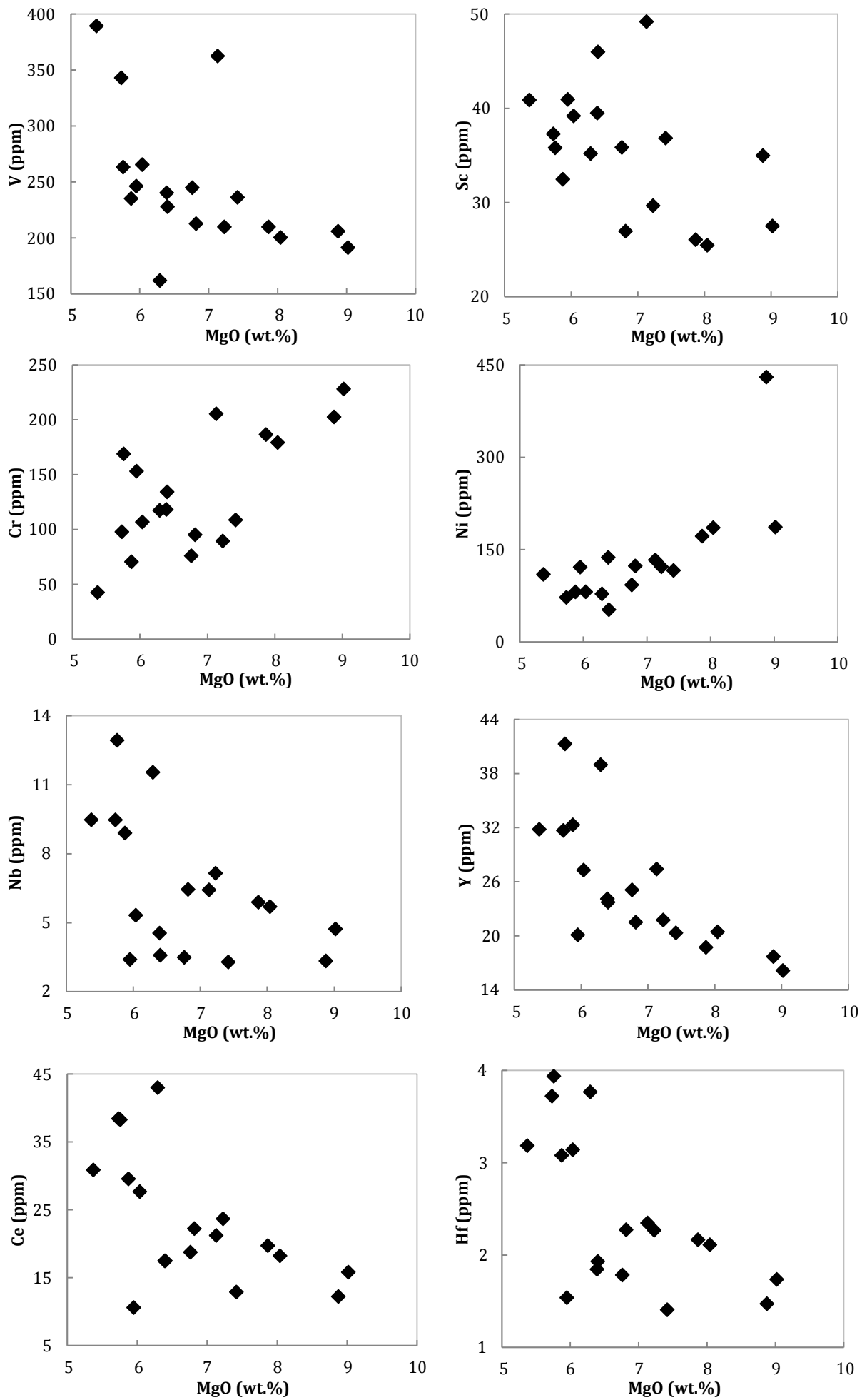
Fig. 4. Bivariate diagrams of selected trace elements vs. MgO for the du Chef dykes.
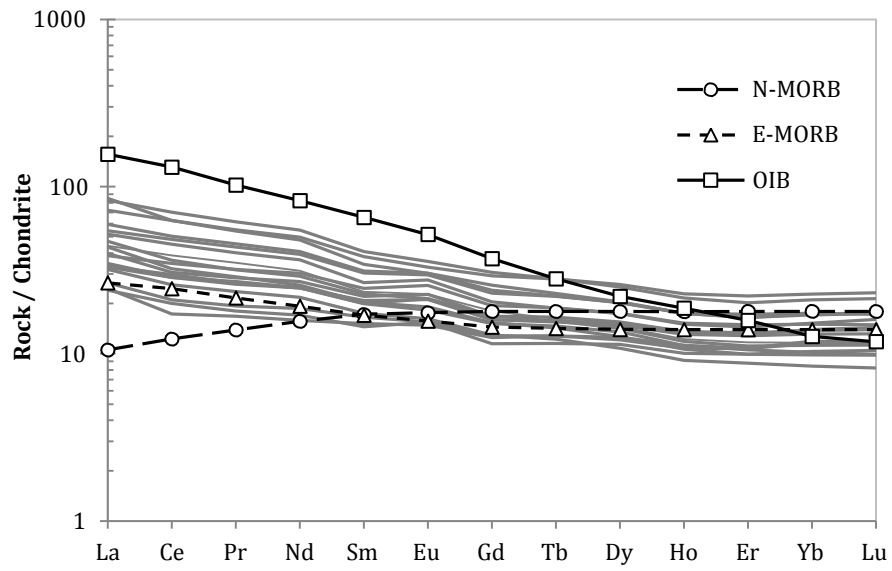
Fig. 5. Chondrite-normalised rare earth element plot of the du Chef dykes (B). End-members and normalising factors from Sun and McDonough (1989).
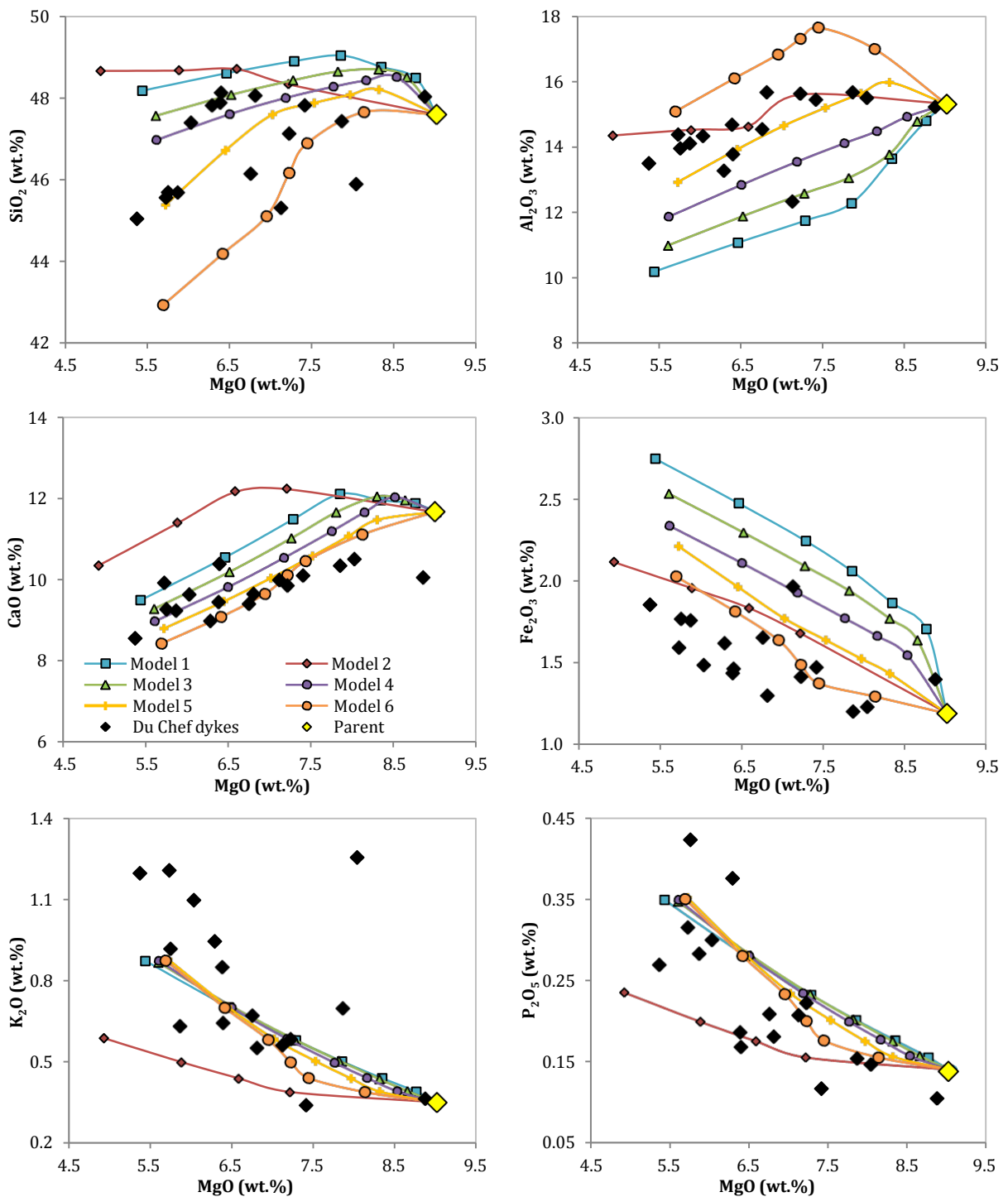
Fig. 6. Bivariate diagrams of selected major elements vs. MgO trends for the du Chef dykes and those predicted by fractional crystallisation of a parent magma with a composition equal to that of sample DC011. Markers on the model lines are placed at intervals of 10% crystallisation.
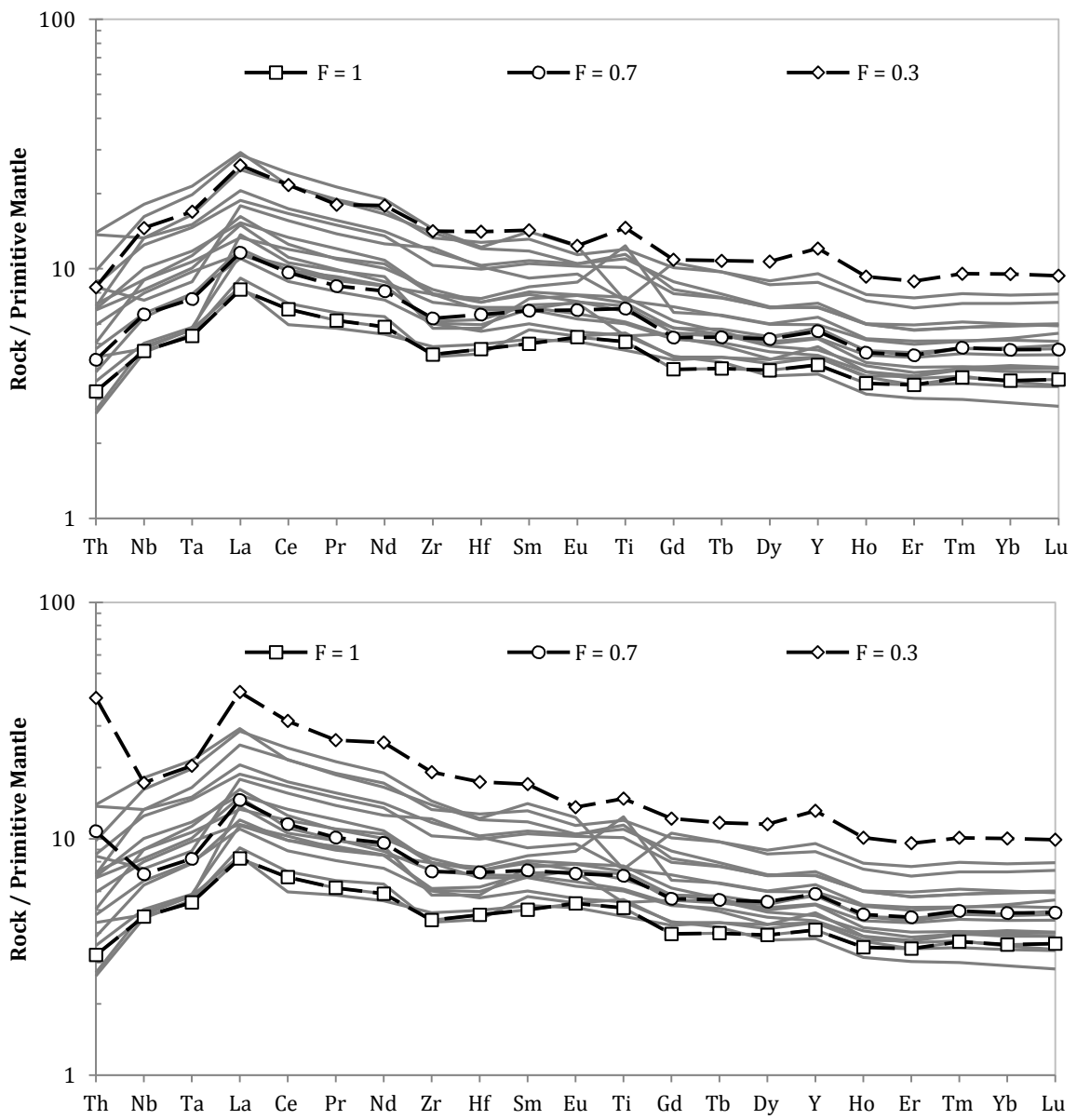
Fig. 7. Primitive mantle-normalised trace element diagrams for the du Chef dykes. Also plotted are the trends predicted by FC (A) and AFC (B) using the starting composition of sample DC011 and the model constraints explained in the text.
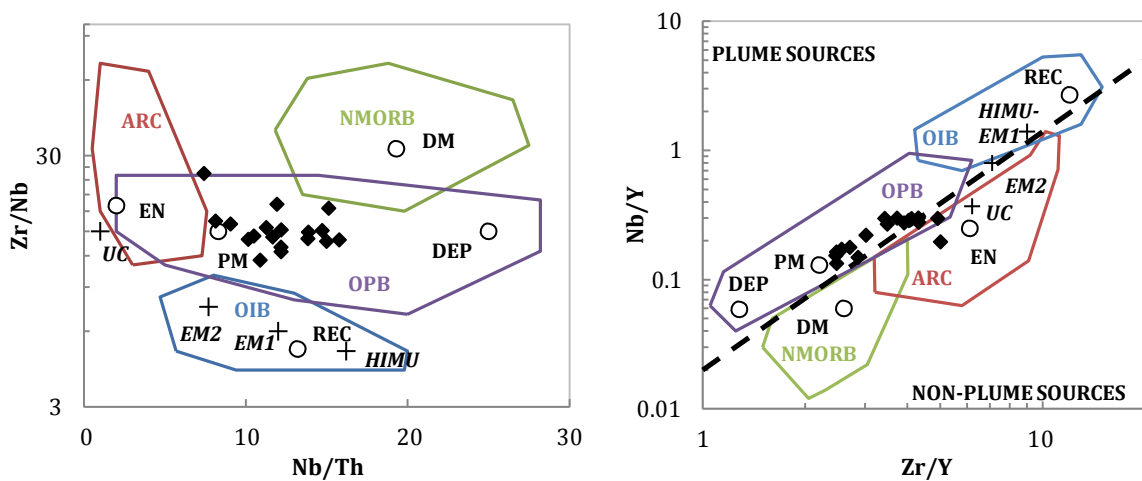
Fig. 8. Zr/Nb vs. Nb/Th diagram (A) and Nb/Y vs. Zr/Y diagram (B) for the du Chef dykes. Field boundaries and end-member compositions from Condie (2005). Abbreviations: PM = Primitive Mantle, DM = shallow depleted mantle, ARC = arc related basalts, NMORB = normal mid-ocean ridge basalt, OPB = oceanic plateau basalt, OIB = oceanic island basalt, DEP = deep depleted mantle, EN = enriched component, REC = recycled component.
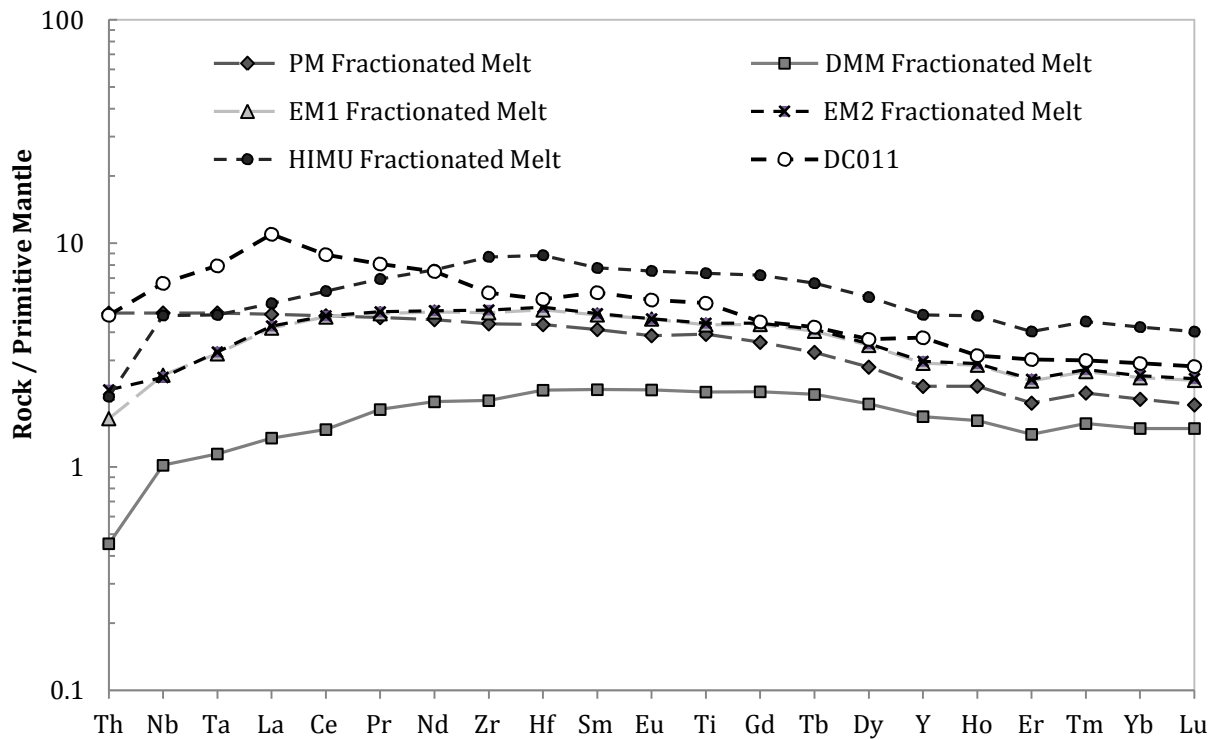
Fig. 9. Primitive mantle-normalised trace element diagrams for the du Chef sample DC011. Also plotted are the trends predicted for magmas which have evolved through 32% fractional crystallisation of olivine, following 30% batch partial melting of garnet lherzolites (Johnston et al. 1990) from the EM1, DMM and PM mantle reservoirs.
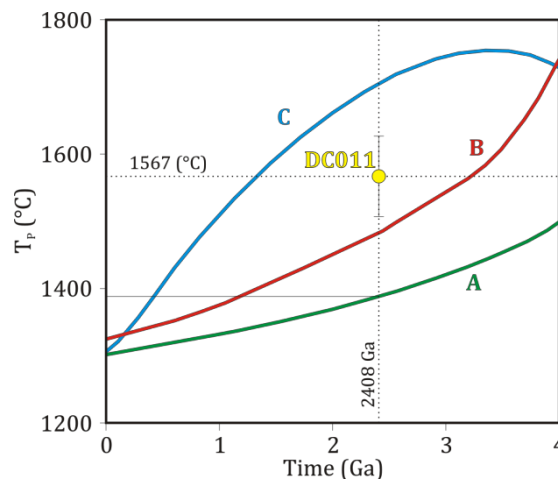
Fig. 10. Temperature evolution of the upper mantle through time using different models; A – Davies (2009); B – Richter (1988); C – Korenaga (2008).
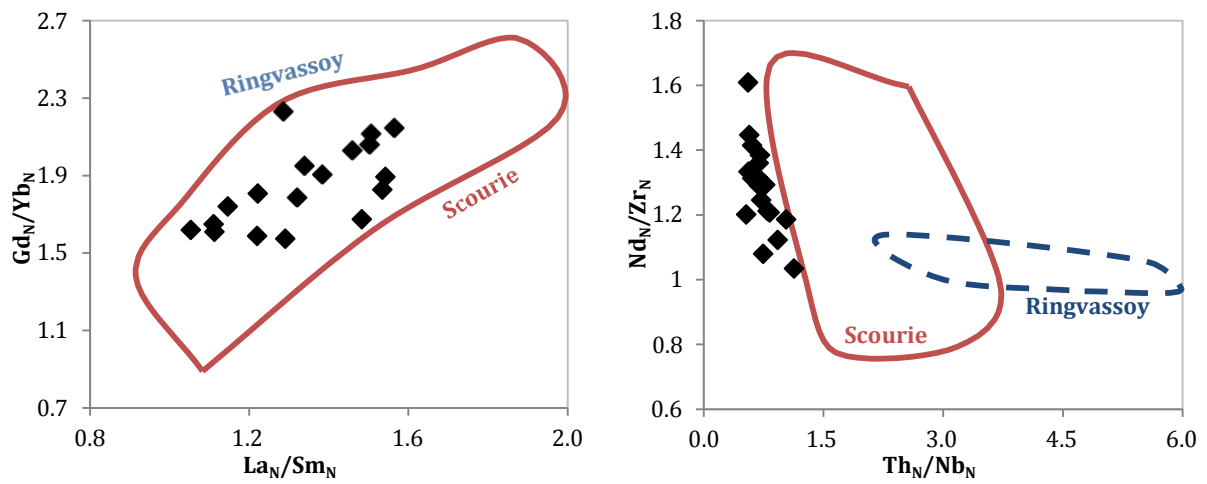
Fig 11. Primitive mantle-normalised bivariate diagrams showing composition of the du Chef dykes, Ringvassoy dykes (Kullerud et al. 2006) and Scourie dykes (Hughes et al. submitted).
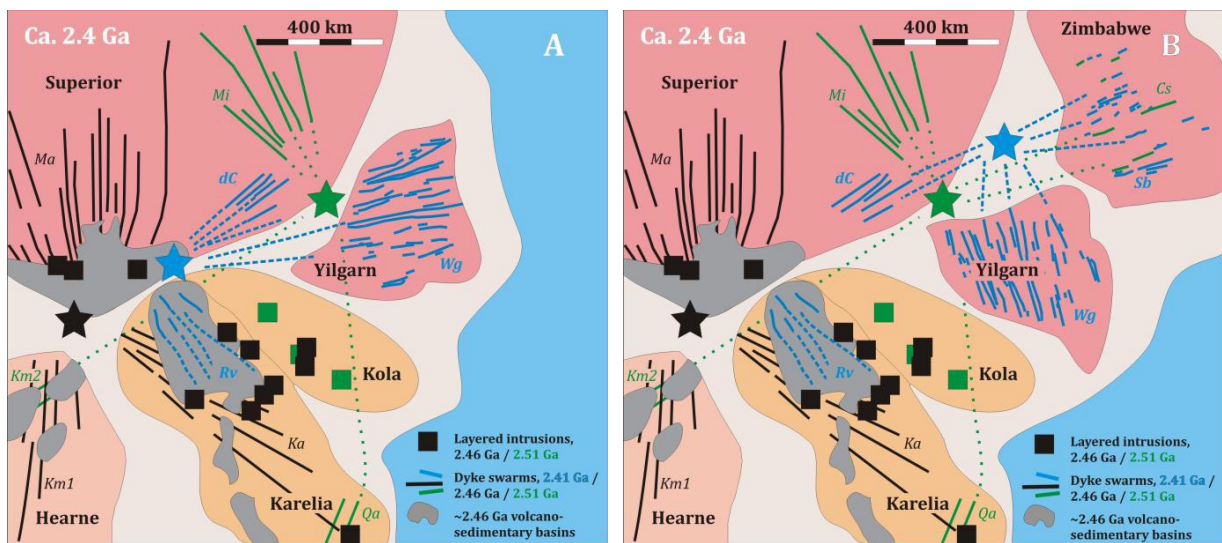
Fig. 12. Ca. 2.4 Ga continental reconstructions showing potential configurations of the eastern margin of Superia. Abbreviations for dyke swarms: Km – Kaminak, Ma – Matachewan, Ka – Karelian, dC – du Chef, Sb – Sebanga, Cs – Crystal Springs, Mi – Mistassini, Qarliit Nunaat, and Rv – Ringvassoy. Modified after Soderlund et al. (2010).

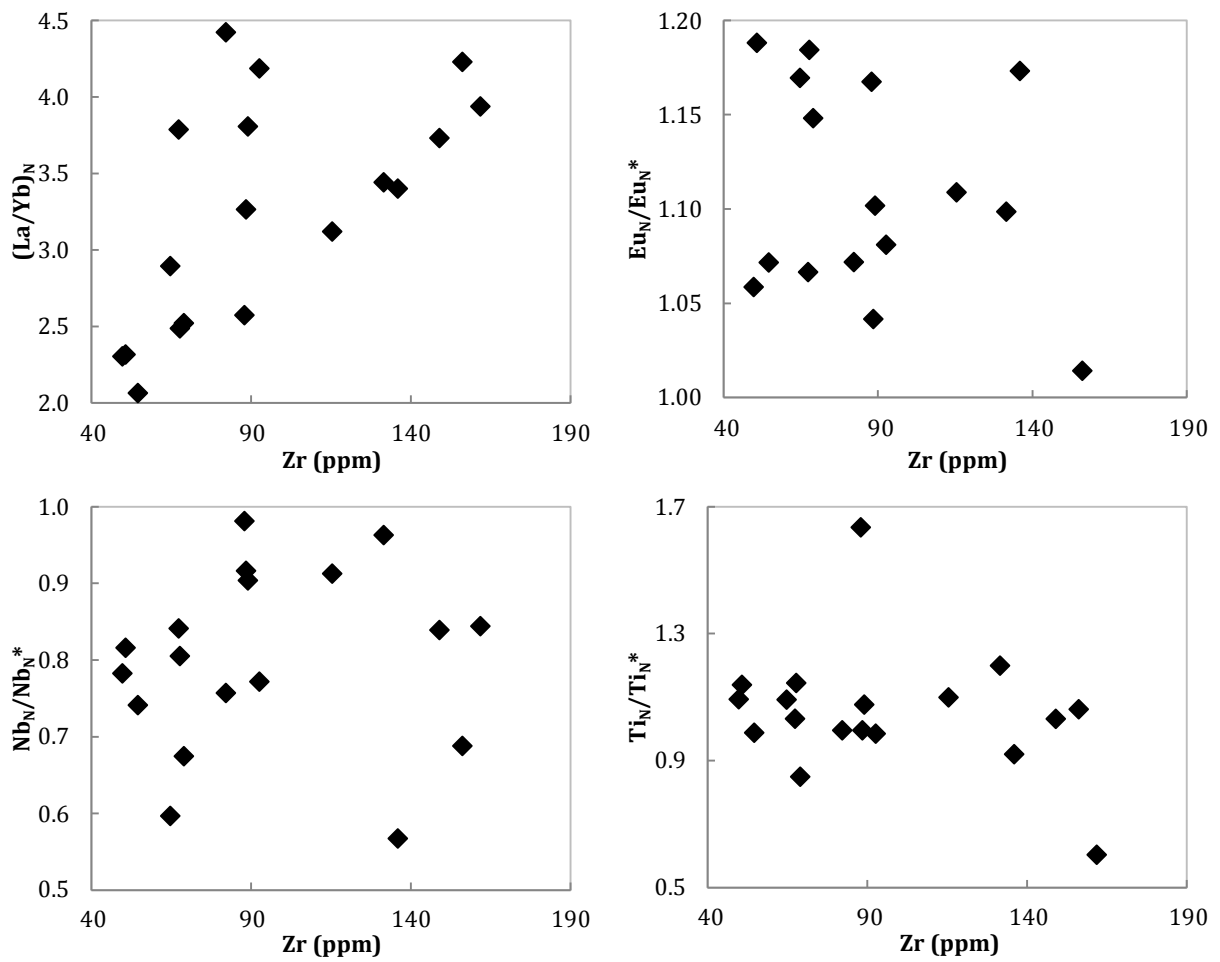**Supplementary Equations**

Supplementary Figure 1. Photographs of the du Chef dykes: A – road cut exposure on highway 167; B – whale-back exposure equivalent to site sampled by Krogh et al. (1984); C – linear contact between du Chef dyke (dC) and the country rock (CR) northwest of the Grenville Front; D – irregular contact between du Chef dyke and country rock from within the Grenville Front; E – garnet-bearing amphibolitised du Chef dyke; F – du Chef dyke with preserved igneous texture.
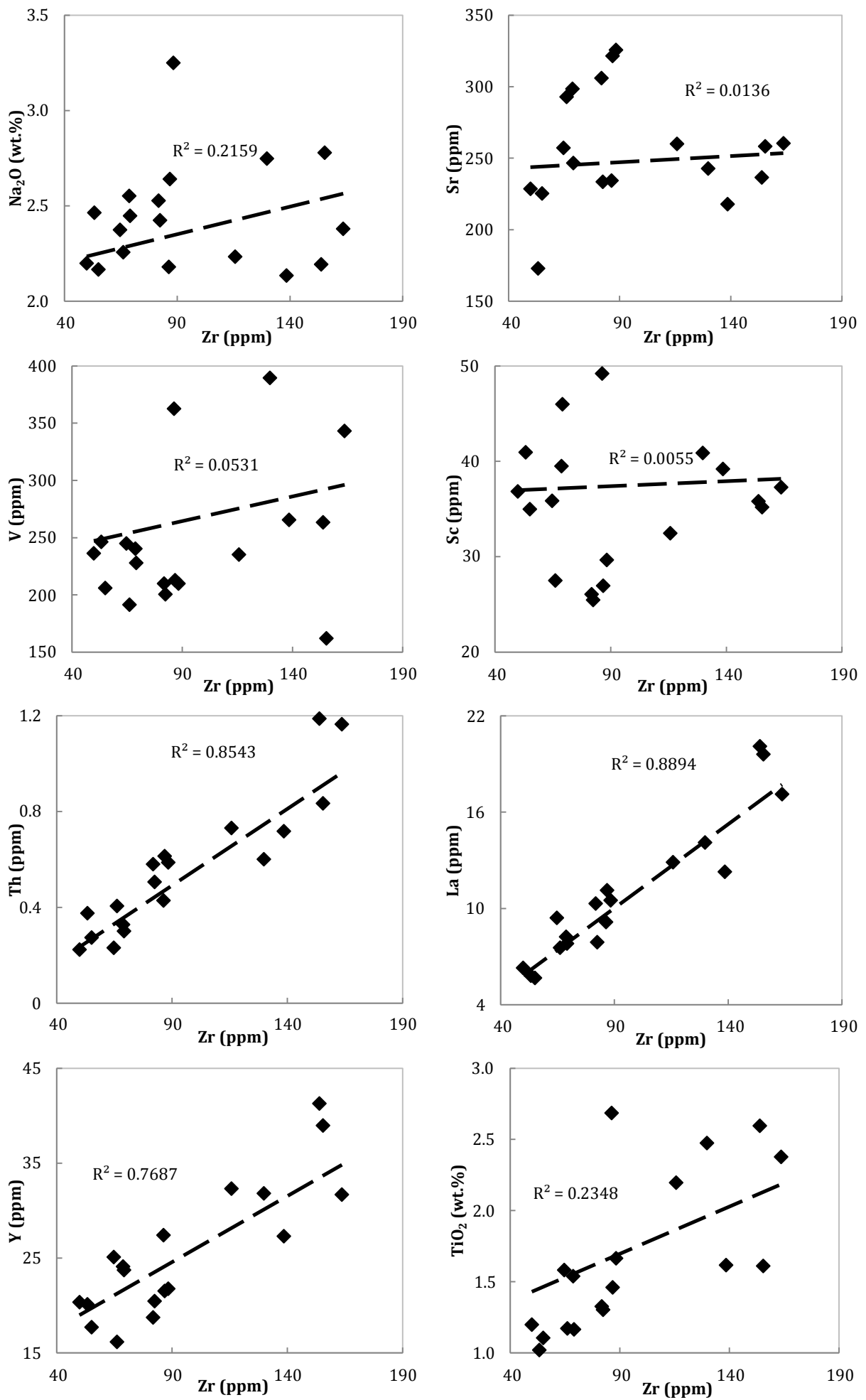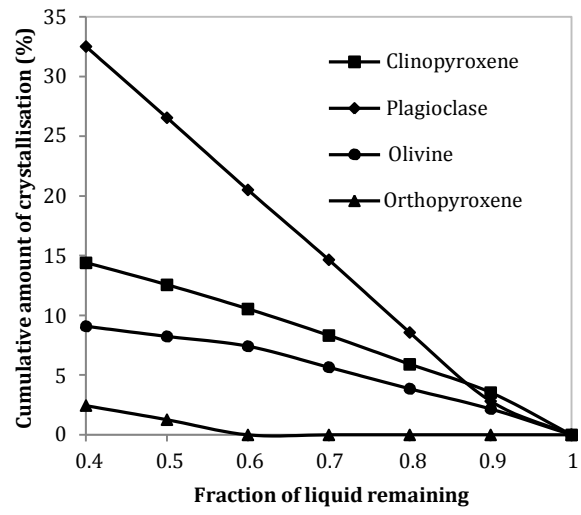
Supplementary Figure 2. Bivariate diagrams of selected elements plotted against Zr for the du Chef dykes.
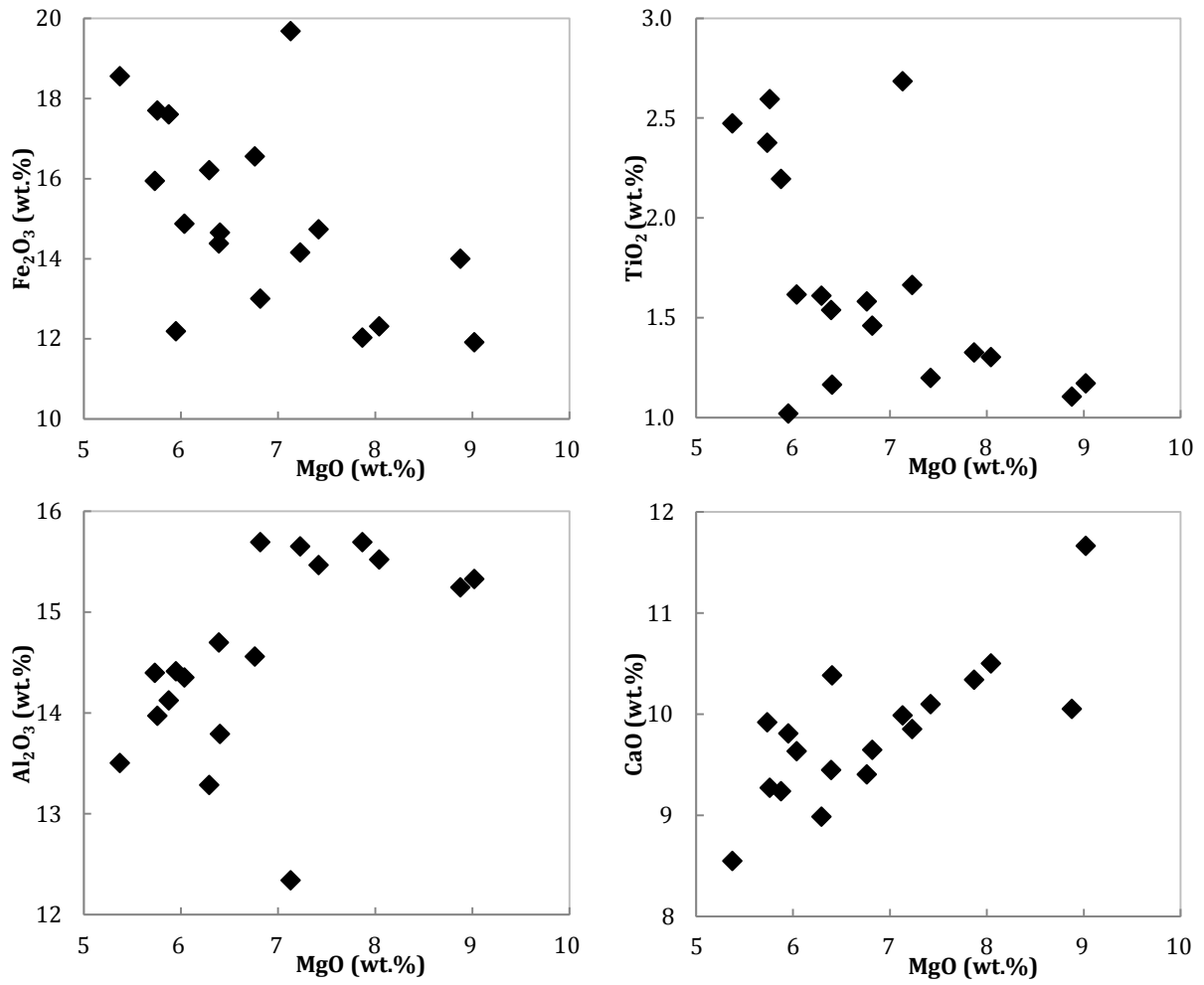
Supplementary Figure 3. Bivariate diagrams of selected major elements vs. MgO for the du Chef dykes.

Supplementary Figure 4. Selected Bivariate diagrams for the du Chef dykes.[Eu$_N$* = (Gd$_N$ + Sm$_N$) / 2; Nb$_N$* = (Th$_N$ + La$_N$) / 2; Ti$_N$* = (Gd$_N$ + Sm$_N$) / 2]

Supplementary Figure 5. Diagram showing the cumulative proportions of crystals formed by fractional crystallisation of the du Chef parent at 10% intervals of crystallisation.